Climate Dynamics
https://doi.org/10.1007/s00382-020-05561-3

Competing aerosol effects in triggering deep convection over the Indian Region

M. G. Manoj[1,2] · Seoung-Soo Lee[2] · Zhanqing Li[2]

Received: 22 April 2020 / Accepted: 25 November 2020

Abstract
Contrasting direct and feedback effects of aerosols on deep convection in the Gangetic Plain of Indian subcontinent have been analyzed by employing observation and modeling framework during the Ganges Valley Aerosol Experiment conducted in 2011. The key question addressed in the current investigation is: while the aerosol direct radiative effect leads to reduced surface shortwave flux and possible stabilization of the lower atmosphere, how is the deep convection favored in a heavily polluted atmosphere? The composites of aerosol, cloud and meteorological parameters during the formation of deep convective clouds (DCCs) under both light- and heavy- pollution conditions are contrasted to elucidate the aerosol effects. An enhanced low-level warming is discernible due to the presence of heavily polluting absorbing aerosols. A seminal role of aerosols in increasing the moist static energy (MSE) through enhancement of internal energy is identified as a primary feature that increases the convection potential of the lower atmosphere. Concomitantly, the greater moisture convergence facilitated by dynamical feedback of enhanced low-level heating destabilizes the atmospheric stratification. Additionally, the microphysical invigoration is examined for any possible role, nevertheless, only a weakened invigoration could be observed possibly due to dominance of meteorology. The observed results are well supported by model simulation of a deep convective event under high- and low-aerosol backgrounds. Besides highlighting the dominance of radiative processes over microphysical processes under heavily polluted environment, the significant correlation between aerosol and high clouds observed during DCC formation under such conditions suggests that the aerosol direct effect in weakening convection could be overcome primarily through enhancement in MSE and concomitant moisture convergence.

Keywords Aerosol · Deep convection · Radiative forcing · Moist static energy · Cloud microphysics

1 Introduction

Accurate representation of the sub-grid scale variability of clouds is essential for climate models (IPCC 2007). However, cloud processes are influenced by nonlinear feedbacks of a variety of dynamic and thermodynamic parameters such as radiation, atmospheric moisture, updraft velocity and cloud microphysics. While environmental conditions are the primary determinant of clouds and convection, aerosols have also been shown to play a significant role in their development (Albrecht 1989; Khain et al. 2004; Rosenfeld et al. 2008; Lee and Feingold 2013; Li et al. 2017a, 2019; Su et al. 2020). The interaction of aerosols with clouds has long been recognized as potentially capable of altering cloud micro- and macro-physics (Bhawar and Devara 2010; Tao et al. 2012; Kaskaoutis et al. 2018). Aerosols affect the climate directly by absorbing and scattering solar radiation, and indirectly by modulating cloud microphysical properties in the form of cloud condensation nuclei (CCN) (Charlson et al. 1992; Babu et al. 2002; Ramanathan and Carmichael 2008; Li et al. 2011; Singh et al. 2018). On short time scales, aerosols can affect fast physical processes to alter cloud and precipitation. On longer time scale, aerosol can affect the intra-seasonal to inter-seasonal monsoon circulation and decadal climate changes especially those linked with the

Supplementary Information The online version contains supplementary material available at https://doi.org/10.1007/s00382-020-05561-3.

✉ M. G. Manoj
mgatmos@gmail.com

[1] Advanced Centre for Atmospheric Radar Research, Cochin University of Science and Technology, Cochin 682022, India

[2] Department of Atmospheric and Oceanic Science & Earth System Science Interdisciplinary Center, University of Maryland, College Park, MD 20740, USA

Published online: 02 January 2021

Asian monsoon systems in China and India (Manoj et al. 2011; Ramanathan et al. 2013; Li et al. 2016; Singh et al. 2019). Modeling studies suggest that the aerosol direct radiative effects could enhance the pre-monsoon precipitation (March through May), but decrease the monsoon rainfall over the Indian subcontinent (e.g., Ramanathan et al. 2005).

Among the various physical processes that aerosols induce, the contrasting role of aerosols in cooling the surface and weakening the convection in the direct way, and invigorating deep convective clouds (DCC) in the indirect way (Andreae et al. 2004; Rosenfeld et al. 2008) is of special interest. This is because these effects suppress or amplify each other depending on the instantaneous state of the atmosphere. Aerosol-induced surface cooling reduces the evapotranspiration in addition to creating a more stable atmosphere in the planetary boundary layer (PBL; Li et al. 2017b), thus enervating the convection potentially. At the same time, more aerosols under fixed moisture content delay the warm rain process (Albrecht 1989). The suppression of warm rain by aerosols causes most of the condensates to ascend, freeze and release the latent heat of freezing before precipitating, and leads to more persistent updrafts and to more vigorous clouds before the precipitation-induced downdrafts take over (Koren et al. 2005; Tao et al. 2007; Rosenfeld et al. 2008). It is also proposed that since smaller droplets freeze at higher altitudes and at lower temperatures, more latent heat is released higher in the atmosphere (Rosenfeld and Woodley 2000), although the invigoration effect was later found to be even more significant for warm clouds under clean environments (Fan et al. 2018). In this manner, aerosols facilitate local convection with stronger intensity. Depending on the environmental conditions and dynamical feedbacks, aerosol net effect on convection and precipitation can be positive, negative or mixed (Chakraborty et al. 2004; Bollasina et al. 2008; Collier and Zhang 2009; Lau et al. 2006). The analysis of Li et al. (2011) has shown that while the microphysical effect is strongest for shallow convective clouds, the invigoration effect is strongest for deep convective clouds. Some simulation studies have confirmed the invigoration hypothesis for deep warm base clouds with weak wind shear in moist environment (Fan et al. 2009). In some cases, no invigoration was obtained, and for cool base clouds, dry environment and/or strong wind shear, the precipitation amount was even decreased (Rosenfeld et al. 2013; and references therein). Some studies (Tao et al. 2007; Lee et al. 2010) have shown that aerosol-induced greater low-level evaporative cooling of the enhanced cloud mass and rainfall produced stronger gust fronts that triggered more new clouds and invigorated them.

Over the past decade, much attention has been given to the aerosol effects on deep convection (Koren et al. 2005; Khain et al. 2005; van den Heever and Cotton 2007; Fan et al. 2009). Deep convective clouds (DCCs) are one of the important components of the Asian monsoon, and play a crucial role in the hydrological and radiative balance of the Earth's climate system (Lee and Feingold 2013). Further, DCCs in the tropics constitute the upward branch of the Hadley cell and provide a conduit through which energy, momentum, moisture, aerosols and chemical species are moved from the boundary layer to the upper troposphere and lower stratosphere (Rafkin 2012). Using the A-train satellite measurements made across the tropical zone, the influences of aerosol on all deep convective clouds have been identified and quantified (Niu and Li 2012; Peng et al. 2016). While being transported, these aerosols, among other numerous factors, act to regulate the precipitation systems including DCCs over this region. Though their frequency of occurrence is rather small, DCCs contribute significantly to the total rainfall. Besides, it is likely to have an overall warming effect ($\sim 0.5\ \mathrm{Wm}^{-2}$) due to the expansion of the anvil coverage by the aerosol invigoration (Yan et al. 2014) that is necessary to close a gap revealed by a recent study of the aerosol effects on marine boundary-layer clouds (Rosenfeld et al. 2019).

Using satellite observations over the Atlantic Ocean, Koren et al. (2005) have shown that the presence of aerosols and the structural properties of deeper and more expansive convective clouds are highly correlated. In the case of deep convection, the CAPE value closely tracks changes in the PBL, and is controlled by boundary-layer temperature and humidity (Donner and Phillips 2003); the source of energy for both convective boundary layers and deep convective cells ultimately comes down to surface heating and moisture (Zhou and Geerts 2013; Medeiros et al. 2005).

The Asian monsoon region is characterized by substantial amount of aerosols originating from both natural and anthropogenic sources (Menon 2004; Ramanathan et al. 2005; Lau et al. 2009; Manoj et al. 2011). Due to population proliferation and rapid socio-economic modernization and urbanization, the resulting anthropogenic emission of pollutants and particulate matter has increased on an unprecedented scale especially in China and India. The Indo-Gangetic Plain (IGP), which is a rapidly developing industrial section bounded by the Himalayas to the north, is the greatest source of both natural and anthropogenic aerosols of the Indian subcontinent. The Indian summer monsoon is a prominent feature of the global circulation, which is also associated with the daily lives of billions of people. The consequence of the aerosol effects on the monsoon environment is manifold (Li et al. 2011). Absorbing type of aerosols, such as soot and mineral dust, has been shown to heat the lower atmosphere, leading to surface cooling. Further, they reduce the low-level clouds by increasing the temperature and reducing the relative humidity, leading to evaporation of cloud droplets (Lau et al. 2009). Some studies have indicated that aerosols may weaken the strength of the Asian monsoon through enhanced

surface cooling and a decrease in the north–south temperature gradient (Menon et al. 2002; Ramanathan et al. 2005; Li et al. 2011).

While the indirect effect delays/inhibits warm rain process and invigorates convection by additional release of latent heat, the direct effect tends to cool the surface and thermodynamically stabilize the lower troposphere (Su et al. 2020). The vertical structure of the PBL, which fuels the convection, is thus modified by the direct effect. The vertical distribution of aerosols, viz., concentration, size distribution, and optical and radiative characteristics, is a major decisive factor of the atmospheric heating which alters the PBL structure and convection (Shamanaev and Kokhanenko 2013; Zhang et al. 2015). Motivated by the importance of the effects of aerosols on clouds and convection, this paper analyzes the contrasting roles of aerosols in strengthening/weakening deep convection over the IGP region during monsoon. We investigate how exactly the direct effect is overcome by a combination of the direct effects, the indirect effects and concomitant feedback processes.

The rest of the paper is organized as follows: the data used and methodology adopted in this paper are given in Sect. 2; Results arising from the analysis and the discussion of the same are produced in Sect. 3. The summary and main findings are documented in Sect. 5.

2 Data and methodology

In the present investigation, the contrasting effects of aerosols on deep convection that occurred nearby the observation site during the Ganges Valley Aerosol Experiment (GVAX) in the Indo-Gangetic Plain (IGP) in 2011 are investigated using satellite, ground-based and re-analysis data sets. The overall objectives of the GVAX campaign were: (i) to acquire essential cloud, aerosol, and meteorological parameters for the study of their climatic effects; (ii) to examine the roles of aerosols in affecting the regional energy balance, climate and atmospheric circulation with a special focus on the impact of aerosols on the Asian monsoon system; (iii) to understand the mechanisms of the aerosol indirect effect under the special conditions of the region (GVAX Science Plan: http://www.arm.gov/publications/programdocs/doe-sc-arm-10-019.pdf?id=95).

We use the aerosol and meteorological (temperature, humidity, pressure etc.) and CCN data from the GVAX Field campaign (http://www.arm.gov/campaigns/amf2011gvax) of the Atmospheric Radiation Measurement (ARM) Program of the U.S. Department of Energy. A major limitation of the past field studies is that the measurements were made over homogeneous atmosphere over the oceans which is relatively clean with smooth topography and lesser variety of aerosol types. However, the GVAX scenario was quite different with measurements over the land where there is a strong interaction between the land and the atmosphere, in addition to varying anthropogenic activities and natural eco-system producing different aerosol types. GVAX campaign was conducted to measure relevant radiative, cloud, convection, and aerosol chemical, physical, and optical characteristics over mainland India in the Ganges Valley during a period of 6–12 months. The aerosols in this region have complex sources, including burning of coal, biomass, and biofuels; automobile emissions; and dust. The present study utilizes the instrument data (especially profiles) at a single station (Nainital). Other than the Radiosonde profiles, aerosol chemical and radiative properties have also been utilized. The scientific instruments for GVAX were deployed at the ARIES High Altitude Observatory at Nainital (79° 27′ E, 29° 21′ N, 1943 m above mean sea level) in the IGP.

In addition, we use the daily aerosol optical depth (AOD) at 550 nm (MOD08_D3.005 Version 5, Level-3 data), cloud optical depth (COD), total column precipitable water content (PWC), liquid and ice cloud effective radius (CER), cloud liquid water path (CLWP), cloud ice path (CIP), cloud ice optical depth (CODice), cloud fraction (CF) and cloud top pressure (CTP) provided by the MODerate resolution Imaging Spectroradiometer (MODIS) onboard the Terra Satellite, available at of $1^\circ \times 1^\circ$ resolution. The aerosol extinction profile at 532 nm is obtained from the Cloud-Aerosol Lidar and Infrared Pathfinder Satellite Observation (CALIPSO) satellite-derived aerosol layer data obtained from the URL: https://www-calipso.larc.nasa.gov/tools/data_avail/index.php?d=2011. Moreover, the daily data of certain meteorological parameters (temperature, horizontal and vertical wind components, specific humidity) and cloud variables such as specific cloud ice water content (CIWC) at pressure levels; and high cloud cover (HCC), surface evaporation, the boundary layer height (BLH), total column ice water (TCIW) and the convective available potential energy (CAPE) have been obtained from the European Centre for Medium-Range Weather Forecasts (ECMWF) Re-Analysis Interim (ERA-Interim Project) data sets. The products are available at a horizontal resolution of $1.5^\circ \times 1^\circ$. We also use the daily UV aerosol index (AI) and total column amount ozone (TCO) from ozone monitoring instrument.

The first part of our analysis aims at identifying DCCs that occurred nearby the observation site for the summer monsoon months of June through September (JJAS) in 2011. DCCs were identified from CTP and COD, primarily based on the ISCCP (International Satellite Cloud Climatology Project) cloud classification criteria proposed by Rossow and Schiffer (1999). The region of study is bounded by a rectangular box spanning an area of $10^\circ \times 10^\circ$ (75–85E, 25–35 N; as shown by the white rectangular box in Fig. 1b) centered around Nainital (circled in black). There were eight DCC cases identified during the

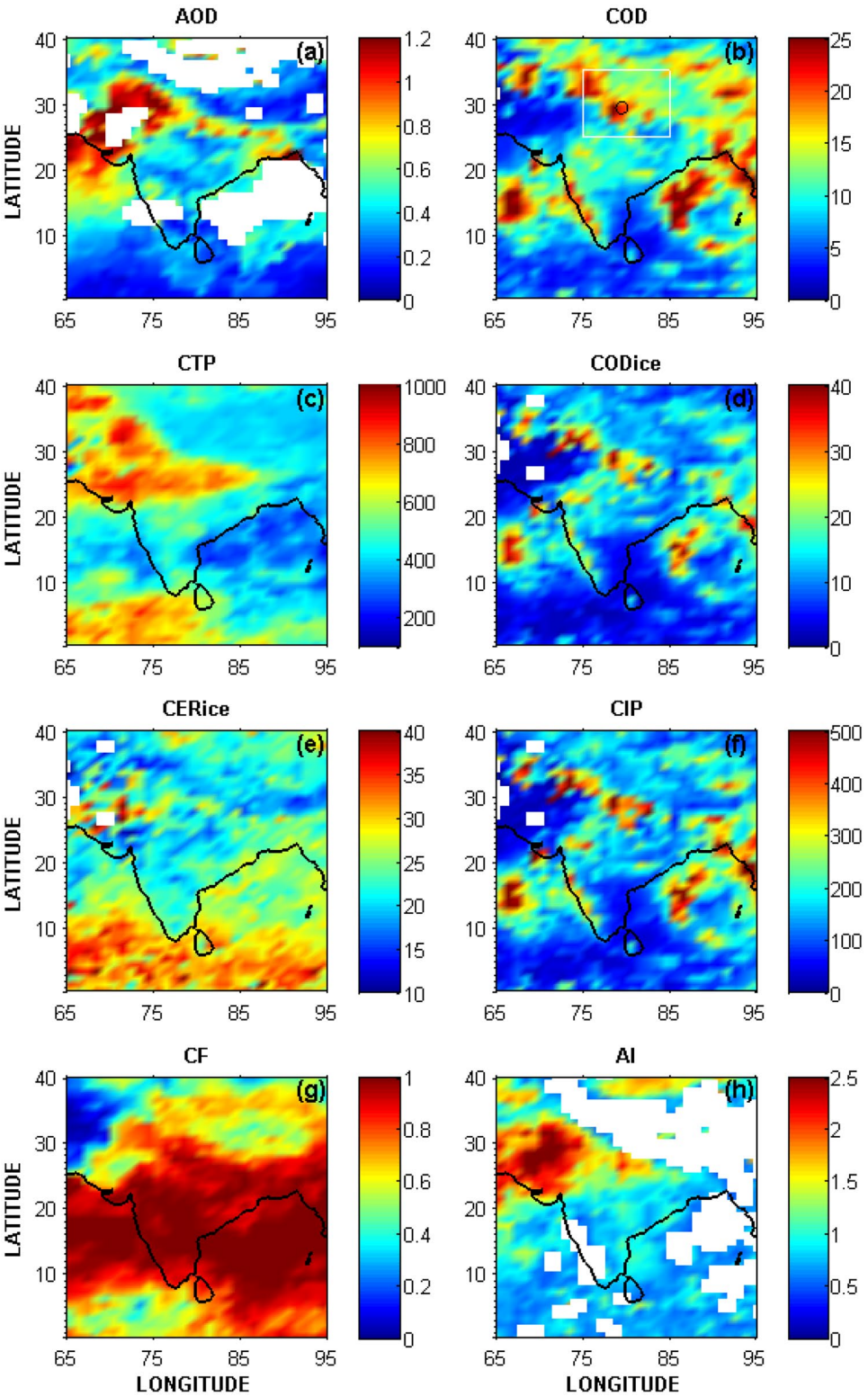

Fig. 1 Spatial pattern of combined HADCC and LADCC composites of **a** AOD, **b** COD, **c** CTP, **d** CODice, **e**CERice, **f** CIP, **g** CF and **h** AI observed during JJAS, 2011

JJAS period: (02 Jun, 07 Jun, 12 Jun,17 Jun, 24 Jun, 15 Jul, 27 Aug, and 16 Sep in 2011) of which eight events were mostly not associated with an active monsoon condition over the core monsoon region as defined by Rajeevan et al. (2010). For studying the impact of aerosol on DCC, we identified those DCCs associated with high (AOD > 0.5) and weak (AOD ≤ 0.3) pollution during JJAS-2011. Thus, the DCCs under High AOD condition (HADCC) events are identified to be during 17 Jun, 24 Jun, 27 Aug, and 16 Sep, and the DCCs under Low AOD condition (LADCC)

cases are during 02 Jun, 07 Jun, 12 Jun, and 15 Jul in 2011. The composites of various cloud and aerosol parameters, and surface fluxes during HADCC and LADCC conditions are constructed to distinguish dynamical and thermodynamical fields to elucidate the role of aerosols in deep convection.

Further, a radiative transfer code, the Santa Barbara Discrete ordinate Atmospheric Radiative Transfer (SBDART; Ricchiazzi et al. 1998) model is used during the high AOD and low AOD events to simulate the representative surface downward and top-of-the-atmosphere (TOA) shortwave (SW) fluxes, and the heating rate (HR) in both polluted and clean atmospheres over Nainital. The input parameters used for SBDART were aerosol parameters like extinction profiles from CALIPSO, single scattering albedo (SSA) from OMI, asymmetry parameter from the global aerosol data set (GADS; d'Almedia et al. 1991; Koepke et al. 1997), in addition to the daily mean TCO and PWC.

Aerosol Radiative Forcing (ARF) is defined as the difference in net fluxes at the surface (SRF) or at the TOA, with and without aerosols (Ricchiazzi et al. 1998; Pandithurai et al. 2004). The ARF is given by the expression:

$$(ARF)_{SRF,TOA} = \left[F_A - F_{NA}\right]_{SRF,TOA}, \tag{1}$$

where $F_{A,NA} = (F\downarrow - F\uparrow)_{A,NA}$, is the net flux with aerosol and without aerosol respectively.

For the atmosphere, the ARF is the difference between that at the TOA and at surface. Thus:

$$ARF_{ATM} = ARF_{TOA} - ARF_{SRF}. \tag{2}$$

Since the detailed information regarding the spectral variation of all aerosol-related parameters was not available over the whole region under study, the radiative forcing calculations were carried out at a wavelength of 0.55 μm with area-averaged aerosol and complementary input parameters. The composite ARF and heating rates were computed at one-hour interval.

Other input parameters for the calculation are the real atmosphere meteorological parameters from radiosonde, the assumed TOA solar radiation, the solar geometry, and the surface reflective properties of a tropical atmosphere. In order to eliminate the contamination of fluxes and HR due to clouds to a certain extent, the same has been estimated by considering the vertical distribution of relevant cloud properties. For this purpose, we have used the mean cloud conditions such as cloud base height, top height, cloud effective radius and cloud optical depth during the cases under consideration. These variables except effective radius were obtained from CALIPSO-derived cloud layer data (Level 2). Representative values of estimated SW fluxes and HR are given for high-AOD DCC (HADCC) and low-AOD DCC (LADCC) cases.

2.1 Weather research and forecasting (WRF) model

For substantiating aerosol effects on DCCs, we use a mesoscale model to simulate a deep convective event. The Advanced Research Weather Research and Forecasting (WRF-ARW) model (version 3.3.1), a three-dimensional non-hydrostatic compressible model, is used here as a cloud-system resolving model (CSRM). A detailed description of the governing equations, numerical methods, and physics of the WRF-ARW model, which is not the WRF-Chemistry (WRF-Chem) model, is documented by Skamarock et al. (2008). Shortwave and longwave radiation parameterizations have been included in all simulations by adopting the Rapid Radiation Transfer Model (RRTMG; Mlawer et al. 1997; Fouquart and Bonnel 1980). The microphysical processes are represented by a double-moment bin-bulk scheme that uses bin-model-derived lookup tables for hydrometeor collection processes. This scheme is developed by Saleeby and Cotton (2004). The details of this scheme are found in Saleeby and Cotton (2004) and Lee et al. (2009). This scheme predicts the number concentration, mass and size of hydrometeors. Note that aerosol effects on the size are a path through which aerosol affects precipitation and cloud radiative properties. Hence, this scheme enables the simulation of aerosol-cloud interactions. Moreover, the bin-bulk scheme adopted here uses realistic collection kernels and terminal velocity, which vary with the varying size of hydrometeors, unlike in other bulk schemes that assume constant collection efficiency and terminal velocity. This enables more realistic simulations of microphysical processes, their variation with the varying size and aerosol effects on the variation in the bin-bulk scheme than in other bulk schemes, thus, grants more confidence to simulations by the bin-bulk scheme than other bulk schemes. In the adopted scheme, a gamma size distribution with fixed breadth is assumed for hydrometeor size distributions. Cloud-droplet and ice-crystal nucleation mimic a size-resolved approach (Lee and Feingold, 2010).

Since we do not have the high spatio-temporal data of all aerosol optical and radiative properties to be fed in to the WRF model, we adopted the simple model (SBDART model whose details are already discussed in the beginning of Sect. 2) which requires data at a single location only.

2.2 Aerosols

We use an observed vertical distribution of aerosol concentrations, depicted in Figure S1, as an initial aerosol profile at the first time step in the control run. Figure S1 shows the initial vertical distribution of aerosol extinction, which is a

measure of the aerosol concentration, and aerosol concentrations. It is assumed that aerosol concentrations do not vary horizontally and they vary only over the vertical domain at the first time step. This variation follows that observed and depicted in Figure S1.

In the present paper, 11% black carbon (BC), and 89% scattering type aerosols (sulfate, nitrate, salt and dust) by mass are assumed to be internally mixed to form aerosol particles (Dey and Tripathi 2007). Prognostic equations are solved to predict the aerosol mass mixing ratio. The aerosol mass mixing ratio is advected, diffused, and depleted by activation and washout by precipitable hydrometeors (i.e., nucleation and impacting scavenging) during simulations. The prognosed supersaturation of air parcele is used to explicitly activate aerosol particles in the adopted bin-bulk scheme; this activation initiates interactions between aerosols and microphysics. After activation, the aerosol mass is transported within hydrometeors by collision-coalescence and removed from the atmosphere once hydrometeors that contain aerosols reach the surface. Aerosols return to the atmosphere upon evaporation or sublimation of hydrometeors that contain aerosols.

The size distribution of background aerosols is assumed to follow that, which is a tri-modal log-normal distribution, in Lee and Feingold (2010). The modal diameter and distribution breadth of each of the modes of the size distribution are assumed to be homogenous in time and space. Hence, aerosol particles at any grid point in the control run have the same assumed shape of the size distribution. Based on the assumed tri-modal log-normal distribution and aerosol composition, the predicted aerosol mass is used to diagnose the aerosol number concentration that varies spatiotemporally due to clouds, advection, and diffusion after the first time step.

The adopted radiation scheme takes the predicted humidity and aerosol number concentrations by other parts of the ARW model, the assumed aerosol size distribution and composition to calculate the optical properties of aerosol particles. This scheme also adopts the predicted hydrometeor size and number concentrations by the bin-bulk scheme and calculates the optical properties of hydrometeors. By using these optical properties, aerosol and cloud effects on longwave and shortwave fluxes and associated radiative forcing and heating rates are calculated by the radiation scheme. Hence, via this radiation scheme, interactions between aerosols and radiation and interactions between clouds, which are affected by aerosols via the bin-bulk microphysics scheme, and radiation are simulated. Here, the optical properties are represented by extinction, single scattering albedo (SSA), and phase function. SSA is around 0.92 at a wavelength of 0.55 μm in this study.

2.3 Case description

Three-dimensional simulation of an observed deep convective event under high AOD (HADCC) case is performed. The simulation is done for 48 h starting on 27 August 2011. The horizontal domain length is set at 100 km in the east–west and north–south direction while the vertical domain length is set at 20 km. The horizontal grid length is 1 km and the vertical grid length is 200 m. Periodic boundary conditions are applied on horizontal boundaries. Large-scale forcings for potential temperature and specific humidity are applied to the model every time step by interpolating the 6-hourly soundings from reanalysis. This method of modeling cloud systems was used for the CSRM comparison study by Xu et al. (2002). Using the Noah land surface model (Chen and Dudhia 2001) with a land surface type, surface heat fluxes are predicted.

The average background aerosol number concentration integrated over the distribution and over the planetary boundary layer is ~ 550 cm^{-3}. To examine the aerosol effect, the control run is repeated but the aerosol number concentration is reduced by a factor of 4. This repeated simulation is referred to as the "experimental run". Figure S1 compares the initial vertical distribution of aerosol concentrations in the experimental run to that in the control run. Table 1 describes the basic setup of physical schemes, aerosol properties and domain for the two runs.

Table 1 Summary of simulations

	Control run	Experimental run
Radiation	RRTMG scheme	RRTMG scheme
Microphysics	Double-moment bin-bulk scheme	Double-moment bin-bulk scheme
Aerosol composition	11% BC and 89% scattering type components	11% BC and 89% scattering type components
Aerosol size distribution	Tri-modal lognormal distribution	Tri-modal lognormal distribution
Initial aerosol concentration	Observed	Four times lower than observed
Horizontal domain length (grid length)	100 (1) km	100 (1) km
Vertical domain length (grid length)	20 (0.2) km	20 (0.2) km

3 Results and discussion

It is well known that the development of deep convection is associated with a multitude of processes that either amplify or partially cancel one another. Among those processes, the present study is focused mainly on aerosol radiative and microphysical processes which had influenced deep convection.

In order to examine the spatial distribution of aerosol and cloud properties, we portray their combined distribution during the LADCC and HADCC cases as shown in Fig. 1 in Sect. 3.1, before going into detailed analysis.

3.1 DCC composites of aerosol-cloud spatial distribution

While moisture availability is a crucial constraint on the development of clouds, we produce the composite picture of various cloud variables including water paths along with aerosol loading in terms of AOD. Figure 1a–h portrays the spatial pattern of DCC composites of AOD, COD, CTP, CODice (ice phase optical depth), CERice (ice phase cloud effective radius), CIP, CF and AI respectively. The white rectangular box in Fig. 1b represents a region of interest. It is noticed that there are high AOD values over the north-western part of the IGP and also around Nainital. In fact, there exists a great range of spatial asymmetry in the distribution of AOD across the country. A maximum value of AOD (of the order of 1.0 or more) has been reported by Ravi Kiran et al. (2009) over the IGP region. However, we do not completely rule out any contribution due to artifact in AOD retrieval by cloud contamination. Nevertheless, IGP is one of the major source regions for various natural and anthropogenic aerosols (Tripathi et al. 2006; Manoj et al. 2012). The region has an uneven topography rising from sea level to about 6 km; having the Thar Desert to the west, Himalayan mountain range to the north and the heavily inhabited plains in the central region; and acts both as preferred center for local convection and barriers to the free flow of air at lower levels (Jai Devi et al. 2011). COD values exceeds 25 over some parts of the region. The CTP shows lower pressure values (< 400 hPa) near the Nainital observatory, indicating deep convective clouds. Further, the ice cloud optical values are also seen to be relatively high, with average CERice values close to 20 around the Nainital region. The CIP and CF are also seen to be high around this region. Figure 1h shows the regional AI values that generally distinguish absorbing aerosols from scattering ones (Hsu et al. 1999). Absorbing aerosol species (BC, smoke, desert dust coated with BC, volcanic ash etc.) decrease the spectral contrast yielding positive AI (Manoj et al. 2011). It is seen that there is a high value of AI observed in and around the IGP region (data missing exactly over the site, but high AI values especially towards the west), which is a clear indication of the presence of absorbing aerosols over the site. Next, we show the mean picture of how the CODice, CERice and CIP vary with an increase in AOD (Fig. 2). It is seen that there exists a positive correlation between AOD and CODice ($r = 0.58$), and CIP ($r = 0.43$) at 90% confidence level (with a sample size, $N = 56$), implicitly suggesting convection favored under increased aerosol loading, considering that negligible correlation was obtained for CERice.

3.2 Thermodynamical response in the PBL and the surface evaporation

Since the presence of light-absorbing aerosols may produce a thermodynamic response in the lower troposphere and in the PBL, we examine the temperature profiles from the available Radiosonde ascents around the occurrence of the DCC cases (i.e., in general, 1–2 h prior to deep convection). It is seen in Fig. S2 that there exist small scale temperature inversions within the PBL on 24 Jun, 27 August and 16 September (~ 0.5 K increase during HADCC cases), and negligible inversions during LADCC cases (07 Jun, 15 July). However, in general, a major distinction is noticed in the surface temperatures, viz., on an average ~ 2 K increase during HADCCs compared to LADCC events, except on 15 July. Since the 2 K additional warming and inversion at the ground could be due to multiple factors, at this stage, it cannot be simply attributed to aerosols alone though we examine the role of aerosols in the following section. Since it is known that aerosols are capable of influencing the PBL through boundary layer thermals, we also examine how the boundary layer heights (BLH) vary during the two events. It is significant to note from Fig. 3a (left column) that the BLH is comparatively high over the region (about 1.5 km around Nainital and crossing 2 km mainly southwest of Nainital) where HADCC developed, as compared to LADCC conditions. In addition, we have compared the BLH value over Nainital with those derived from Radiosonde data (after Sawyer and Li 2013), and it is seen that the BLH from both the methods agree reasonably well within their respective limitations (Figure not shown). The composite BLH difference between the two categorical events is more than 100 m as evident from the rightmost panel of Fig. 3a. However, it should be noted that there are places where PBL shallows within the white box in the right panel of Fig. 3a. The increased values during HADCCs (compared to LADCCs) are observed mainly towards the southwest of the site while decreased values mostly towards slightly northwest, and southeast. This deepening of BLH is a major aspect of deep convection in the tropics as pointed out by Rochetin et al. (2014). In fact, this study has shown

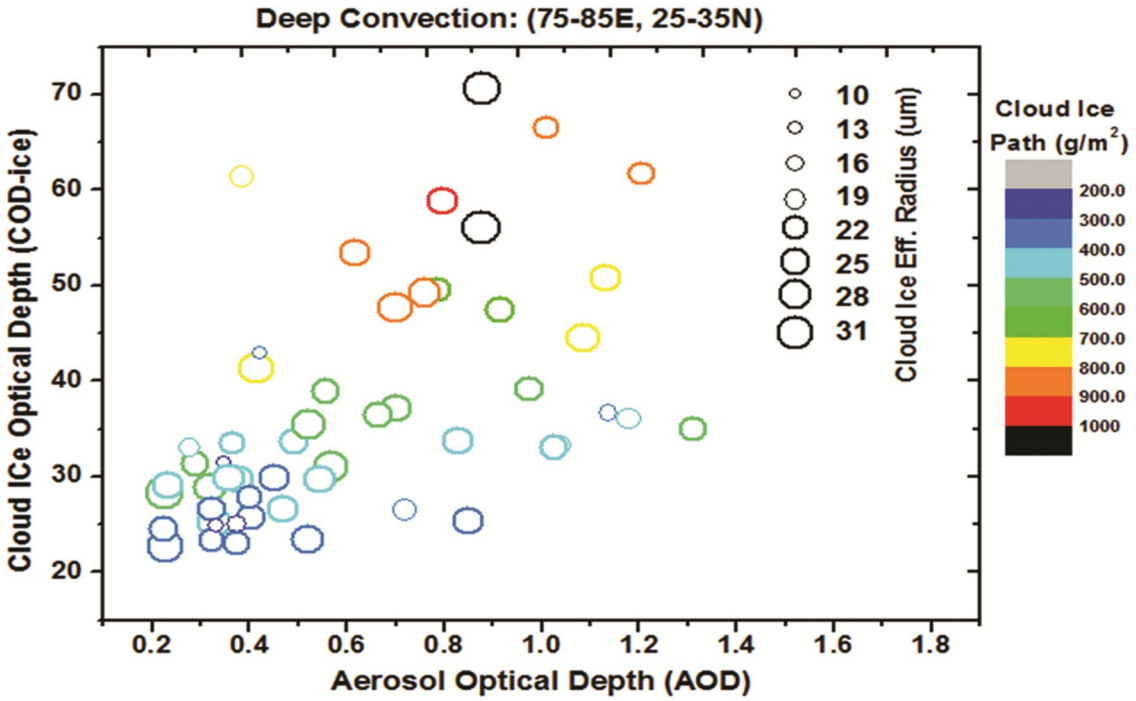

Fig. 2 Scatter plot of AOD versus CODice and CERice for deep convective clouds during JJAS 2011

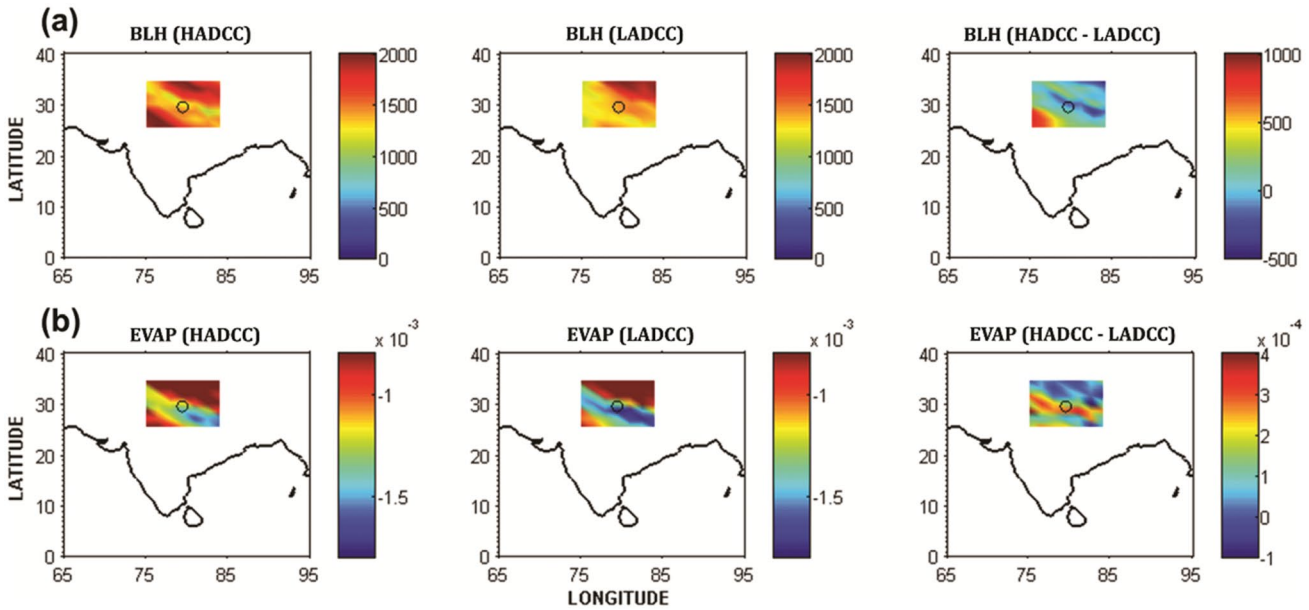

Fig. 3 Composites of spatial pattern of **a** BLH in meters for HADCCs, LADCCs, and difference in BLH between HADCCs and LADCCs. **b** Same as **a** but for the surface evaporation, in units of m of water equivalent

that triggering of convection is driven by evolving properties of the strongest boundary-layer thermals. By combining Fig. S2 and 3a (i.e., enhanced surface temperature together with increased BLH), we consider the favorable condition for enhanced loading of aerosols in the PBL, and its plausible influence in the deepening process but in a qualitative sense. Additionally, it has long been proposed that due to aerosol thermal effect, the surface evaporation may get affected and this aspect is examined through Fig. 3b. The evaporation is reduced, but marginally, during HADCCs as opposed to

LADCC (Evaporation is represented by negative values per data-convention). We attribute a part of this reduction to aerosol direct effect as evident from the discussion below.

3.3 Aerosol radiative forcing and heating rate of the atmosphere

The available vertical profiles of aerosol extinction coefficient were derived for the high-AOD and low-AOD cases. An increase in extinction values is noticed in the first 5 km of troposphere, especially in the PBL (Fig. S3(a)) for high-AOD against the other. These vertical profiles were included in a plane parallel radiative transfer model (SBDART) to simulate the TOA and surface forcing in addition to aerosol-induced heating rate.

The estimated fluxes show that the ARF was much higher during the HADCC with a composite surface forcing of $-49.35\ (\pm 14.77)\ \mathrm{Wm}^{-2}$, compared to a smaller value of $-7.48\ (\pm 3.58)\ \mathrm{Wm}^{-2}$ during LADCC case. The resulting atmospheric forcing was found to be $+43.81\ (\pm 16.1)\ \mathrm{Wm}^{-2}$ and $+5.38\ (\pm 1.7)\ \mathrm{Wm}^{-2}$ for high-AODs and low-AODs, respectively. At this point, it is worthwhile to see the reduced surface evaporation discussed in the previous section, and we argue that the enhanced aerosol-driven surface cooling could be one of the reasons for the reduction in evaporation during HADCCs. The estimated value of atmospheric forcing suggests the significant role played by the relatively high absorbing type of aerosols during HADCC periods over the study region. The resultant aerosol-induced HR profiles (Fig. S3(b)) show a decreasing trend with height in the lower atmosphere (noticeably up to about 3 km, in line with the aerosol extinction) with a slope remaining approximately constant towards higher heights. It is noted that the composite HR at the surface is about 1–2 order of magnitude higher than that during LADCC cases. Even at around 2 km, the HADCC HR value is almost thrice higher than its counterpart. This has a significant impact on the boundary layer dynamics during DCCs under high pollution. It is interesting to compare the HR profile with the corresponding temperature profiles shown in Fig. S2, and we believe that a part of the inversion strength could be explained based on the heating produced by aerosol forcing. This being the case regarding the direct effect of aerosols on surface fluxes and evaporation on one hand, we try to find out what consequences are expected out of this thermal forcing on the other hand, especially in the form of moist static energy and dynamical response.

3.4 Moist static energy and dynamical response

It is well known that the formation and growth of clouds and precipitation are associated with phase change of water. For deep convection, the lower troposphere heating and moistening are highly essential (Wu and Deng 2013). Thus, it requires the consideration of temperature as well as moisture, feasibly expressed in a single quantity, phrased as the moist static energy (MSE). During convection, the MSE is vertically rearranged; however, the vertically integrated MSE is not significantly affected, and it is a useful parameter that is approximately conserved during adiabatic motions (Back and Bretherton 2006). The MSE can be defined as:

$$MSE = C_p T + gz + Lq, \tag{3}$$

where T is temperature, C_p is the specific heat at constant pressure, z is height, g is the gravitational acceleration, L is the latent heat of vaporization at 0 °C, and q is the specific humidity (Maloney 2009). The first, second and third terms on the right-hand side (RHS) of Eq. (3) correspond to the internal, potential and latent energy, respectively. For tropical deep convection, the low-level moist static energy build-up is necessary and this build-up is controlled by the corresponding low-level moisture and temperature (Wu and Deng 2013).

Since aerosols change temperature in the lower atmosphere, it is expected that this thermal forcing could alter the internal energy (IE) directly, the latent energy (LE) indirectly, and hence the MSE eventually. In Fig. 4a–c, we analyze the change in IE, LE and MSE, respectively, in the PBL (750 hPa level) during HADCC conditions, and compare them with LADCC cases using the ERA-Interim data. Their differences between the high-AOD and low-AOD events are produced in the corresponding right column. From Fig. 4a, it is seen that, to the region south and southwest of Nainital (represented by the 'O' mark), the IE is greatly enhanced for HADCC cases. Same pattern is observed for LE and MSE (Fig. 4b, c). Interestingly, it is noted from Fig. 1a that the AOD is high over the same region where MSE is increased. Additionally, Fig. 1h reveals that this region is dominated by absorbing aerosols. It is also worthwhile to note that the north and north-eastern regions of the box, which have comparatively less aerosols and having low AI values, correspond to low IE, LE and thereby MSE. Since Nainital lies in the Continental Trough Convergence Zone (CTCZ Science Plan 2011) region, the background dynamics is favorable for low-level convergence and cyclonic vorticity. It is well known that a key factor in aerosol-induced convection is the alteration in thermodynamics. Though it is expected that the vertical stability is increased due to local heating, the resulting spatial asymmetry (noticeably meridional gradient) in heating could compensate for this stabilization. The thermodynamical response analyzed through MSE (Fig. 4c) arises primarily from LE (Fig. 4b); however, there is also a considerable contribution from the IE (by about 100 J kg^{-1} more during HADCCs conditions; Fig. 4a). The composite LE value during HADCC conditions is close to 2.4×10^5 J kg^{-1},

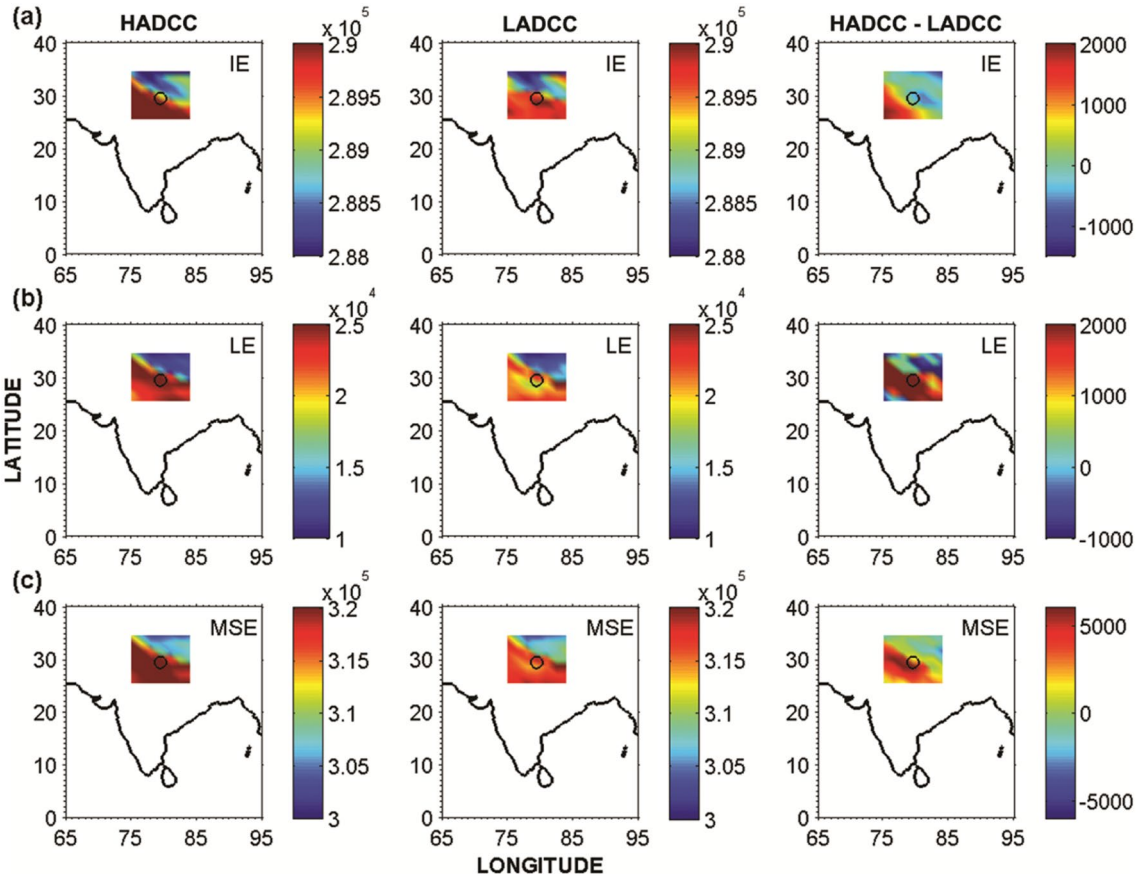

Fig. 4 Composites of the spatial pattern of **a** internal energy (IE) in J kg^{-1} for HADCCs, LA-DCCs, and difference in IE between HADCCs and LADCCs. **b** Same as **a** but for latent energy (LE) and **c**, for moist-static energy (MSE). The location of Nainital is marked by 'O'

while that during LADCCs is 2.38×10^5 J kg^{-1}. It is evident from literature that aerosol-induced heating facilitates significant moisture convergence (Lau et al. 2009; Manoj et al. 2011). The added moisture availability leads to higher release of latent energy in a convective storm. These aspects are evident from Fig. 4a, b, where it is seen that the both IE and LE are significantly higher during HADCC conditions, but with IE one order higher than the LE. Using an interactive aerosol climate model, Wang et al. (2009) have shown that the absorbing anthropogenic aerosols could affect the moist-static energy in the sub-cloud layer, helping a northward shift of the summer monsoon convective precipitation. Based on the discussions here, and the observations in Sects. 3.1 through 3.4, we argue that the enhanced loading of absorbing aerosols is thus playing a significant role in the initiation of deep convection through perturbation in the MSE. Thus, it is expected that the moist static energy build-up expedites deep convection in a destabilized atmosphere, as opposed to the proposed stabilization effect.

The evolution of clouds depends upon a host of processes, mainly those governing the distribution of water vapour (IPCC 2007). Consequent to the thermal constraint as explained above, there could be dynamical response in the region associated with aerosol-induced warming. The heating, however, may induce rising motion, enhance low-level moisture convergence and, hence, contribute to convection positively in HADCC cases. Hence, we now construct the vertical composite of moisture convergence (MC) over the region which is essential for sustained deep convection. Moisture convergence is given by

$$MC = -\left[\frac{\partial(uq)}{\partial x} + \frac{\partial(vq)}{\partial y}\right]. \tag{4}$$

Here, 'u' and 'v' are the horizontal components of wind, and 'q' is the specific humidity. Figure 5 shows the MC for the HADCC and LADCC cases, which clearly indicates enhanced MC at lower levels (PBL) for the HADCC cases. The increased MC at lower levels would lead to a moist unstable atmosphere (through the change of equivalent potential temperature in the vertical, $d\theta_e/dz$). Further, this increased moisture flux will be lifted to upper levels due to (i) enhanced rising motion facilitated by aerosol-induced heating and (ii) reduced density realization, which leads to

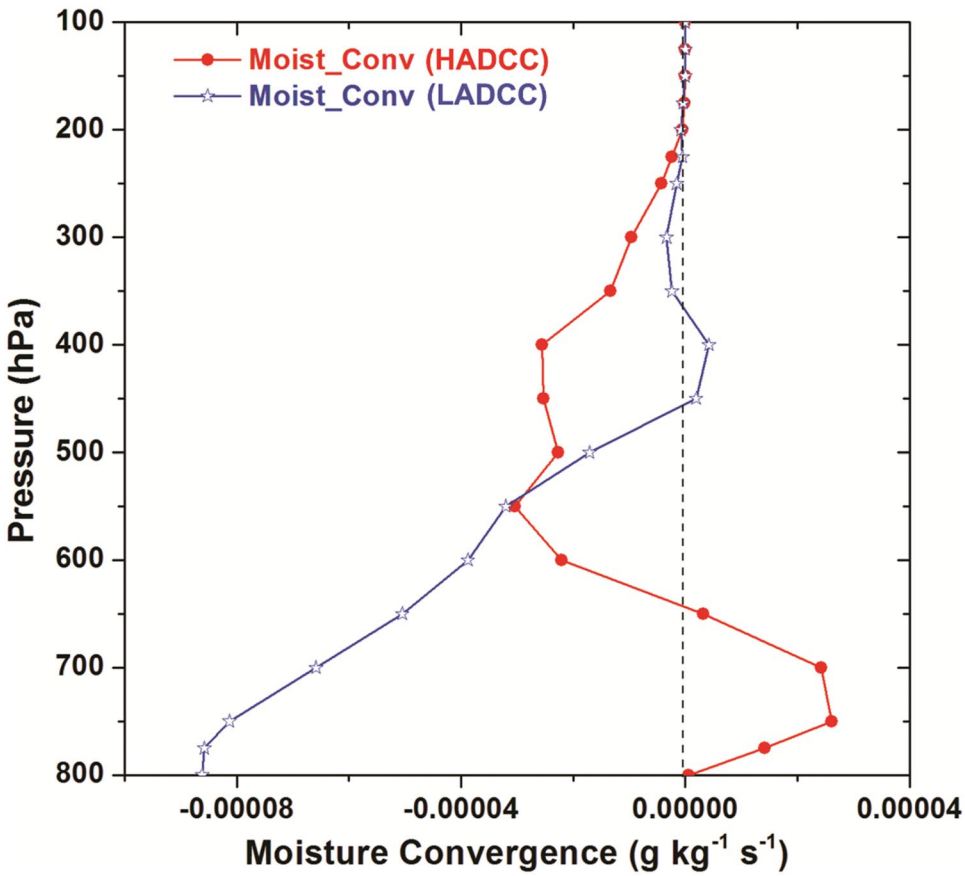

Fig. 5 Composite of vertical profiles of moisture convergence for HADCCs and LADCCs

additional rainfall. It is expected that the latent heat release from enhanced rainfall may excite feedback processes in the large-scale circulation, subsequently amplifying the initial response to aerosol heating, and producing vigorous convection. Thus, the initially subtle stability could be overcome. Using a general circulation model, Manabe et al. (1970) showed that switching off of moist convection in GCM greatly affects the dynamics. Though the bulk circulation features were present in all their simulations, the strength of the Hadley Cell was greatly reduced in the dry simulations and the trade winds were dramatically reduced. The result implies the significance of the interaction between moist dynamics and thermodynamics.

The above discussion is well supported by the fact that an increase in atmospheric temperature increases its water-holding capacity in the PBL (IPCC 2007); a unit rise in temperature increases the water holding capacity by about 7% (as per Clausius–Clayperon equation; Hess 1979; Berg et al. 2013). In addition, since the moist air has less density than the dry air, this expedites the transition to an unstable atmosphere. Our observations show that this is happening at lower atmosphere, which also means more moisture available for convection. As a dynamical consequence of the low-level convergence, the lifting is naturally amplified.

3.5 The role of indirect effect and possible invigoration

It is worthwhile to examine the aerosol effect on microphysics during deep convective episodes. We do a preliminary analysis to check the following aspect: how does the indirect effect work during HADCC conditions in combination with the direct effect of stabilization, in a significantly polluted environment? As the central notion of invigoration theory rests on the suppression of warm rain (Andrea et al. 2004; Rosenfeld et al. 2008), and the CCN concentration was much higher for HADCC cases than for LADCC cases (as evident from Fig. S3(a)), the aerosol indirect effect (AIE) was estimated using the MODIS data to check for any change in warm cloud effective radius (r_e) with aerosol loading (in terms of AOD) under fixed CLWP bin. The CLWP, ranging from 1 to 500 gm^{-2}, was binned into an equal interval of 25 gm^{-2}. The AIE for each bin is evaluated using the expression given by Feingold et al. (2001) as:

$$AIE = -\frac{\tau_a}{r_e}\frac{\Delta r_e}{\Delta \tau_a} = -\frac{d\ln r_e}{d\ln \tau_a}. \quad (5)$$

Expression (4) portrays the relative change in (r_e) for a relative change in AOD (τ_a). Furthermore, a positive

value of AIE signifies a decrease in effective radius with an increase in AOD (Twomey effect), while a negative value of AIE signifies an increase in effective radius with an increase in AOD (anti-Twomey effect). Analysis was performed for each $1^\circ \times 1^\circ$ box of the study region, and the representative AIE values have been plotted for HADCC and LADCC cases in Figs. S4a and S4b, respectively. It should also be mentioned that a two-tailed student's *t*-test was performed to check the statistical significance of these values at 5% significance level. Subsequently, significant values are shown as red bars and non-significant values by blue ones. Since the number of samples greater than 150 g m^{-2} was significantly less, we show the AIE values for the first six bins only. It is seen that while the LADCC cases were associated with a much stronger and intermittently significant anti-Twomey effect for most of the bins (Notice the averaged negative values of AIE, i.e., − 0.21, − 0.23, − 0.12 which are significant in the first three LWP bins, respectively, provided in Fig. S4(b)), the HADCC events were marked by non-significant and negligible AIE (intermittent cases of Twomey and anti-Twomey effects, i.e., − 0.053, − 0.01, − 0.09, respectively, for the first three LWP bins as evident in Fig. S4(a)) compared to LADCCs. This could be due to competing roles of aerosol microphysics versus meteorology. Though not frequent for all the events compared to LADCCs, the weak anti-Twomey effect hints to the possibility of a suppression of warm cloud droplet growth. This might lead to more cloud water to be lifted up, which is further evident from the vertical profile of enhanced cloud ice water content at upper levels for HADCCs in contrast to LADCCs (Fig. 6a). These additional condensates freezing at upper levels could release more latent heat, which could further intensity the updrafts as illustrated by Fig. 6b where the composite vertical velocity for HADCCs shows a many-fold increase at middle and upper levels. Since the column-integrated ice water (TCIW) is much higher for the HADCCs (Fig. 7a), the CAPE values also show a corresponding increase (Fig. 7b) leading to amplified convection supported by the increased fraction of high cloud cover (HCC; Fig. 7c). Yet, it is cautioned that, the entire changes in any of the above parameters may not be attributed to microphysical processes alone as there could be significant contribution from radiative processes and interactions with the meteorology.

4 Model simulation

4.1 Aerosol effect on sensible heat flux

The surface energy budget represents the exchange of energy between the land surface and the atmosphere, and is strongly impacted by the incoming solar radiation (Steiner et al. 2013). The radiation absorbed at the surface (R_n) is stored in surface elements (represented by ground heat flux—G), and

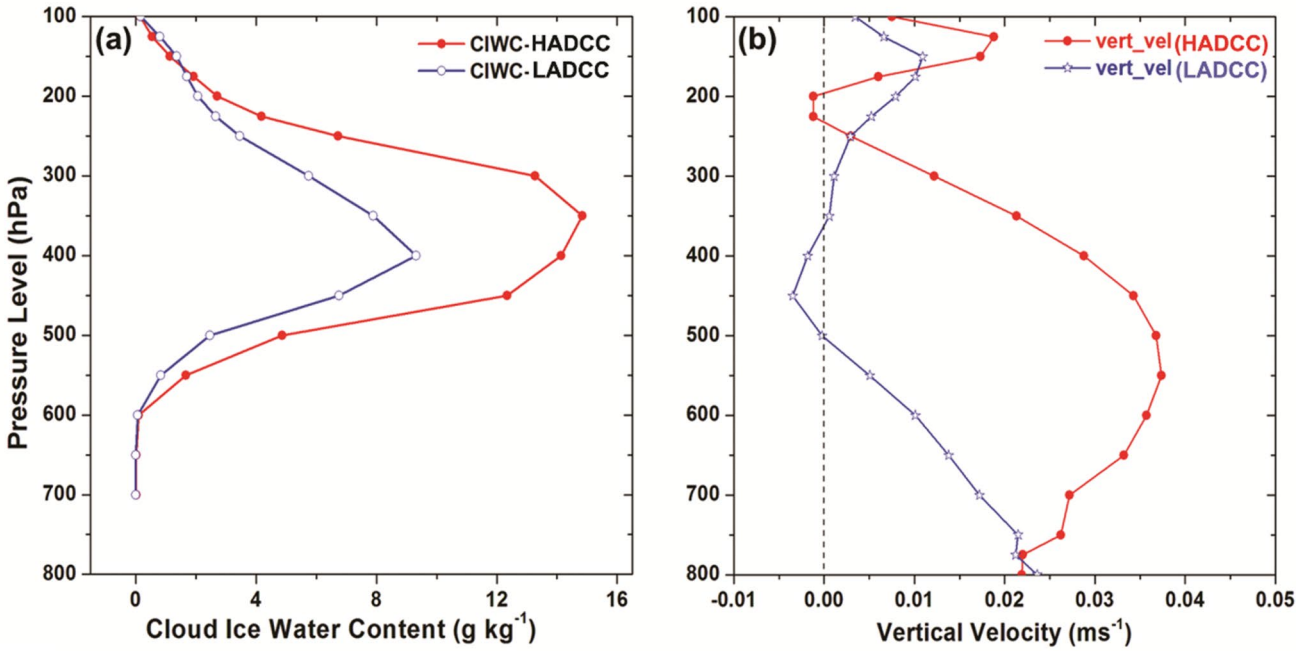

Fig. 6 Vertical composites of **a** cloud ice water content (g kg^{-1}) for HADCCs and LADCCs. **b** Same as **a** but for vertical velocity

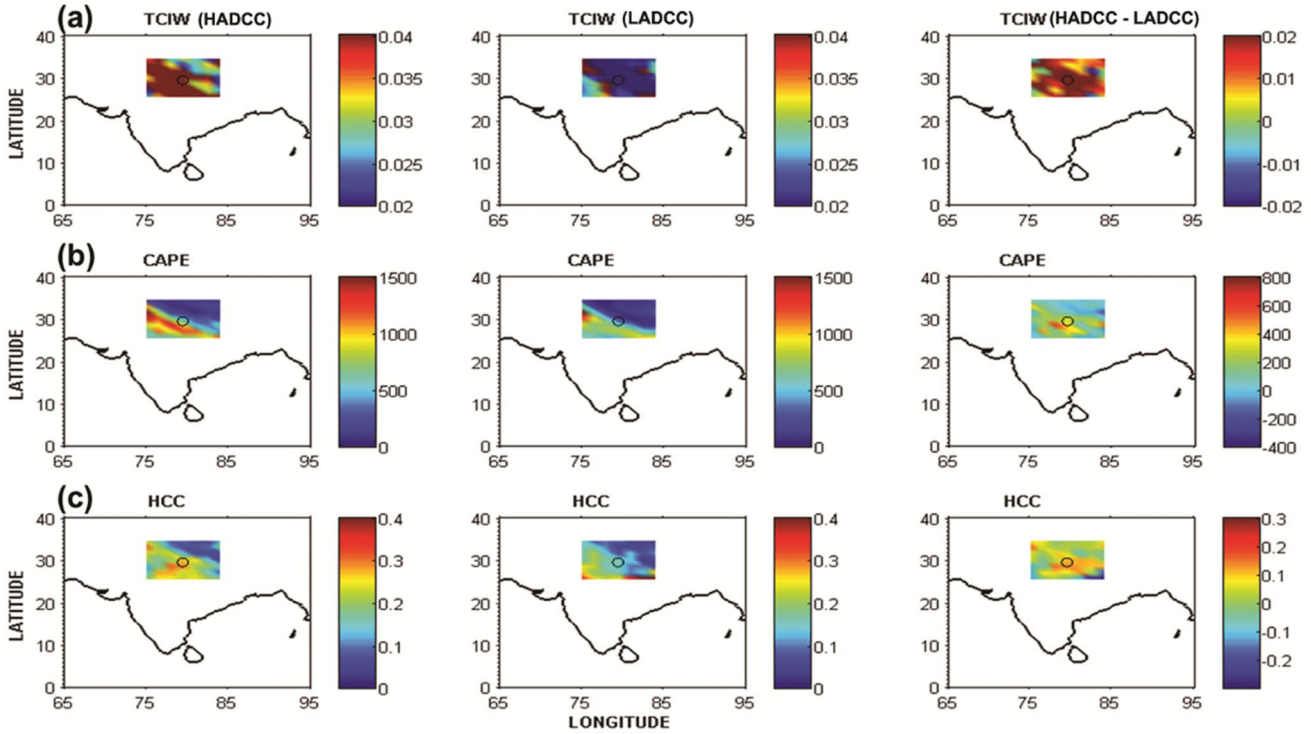

Fig. 7 Composites of spatial pattern of **a** TCIW in kg m^{-2} for HADCCs, LADCCs, and difference in TCIW between HADCC and LADCCs. **b** Same as **a** but for CAPE (in J kg^{-1}), and **c**, for high cloud fraction (HCC)

transported into the atmosphere via sensible (H) or latent (L) heat fluxes, which is expressed as:

$$R_n - G = H + L. \tag{6}$$

The surface fluxes exert thermal forcing to the lower boundary of the atmosphere, and influence meteorological processes including atmospheric stability, cloud development, and precipitation (Stull 1988). Atmospheric aerosols can interact with the solar radiation and reduce the amount of solar energy reaching the surface. The direct effect of aerosols in modifying the sensible heat and latent heat, and thereby influencing atmospheric stability has not been elucidated much in the literature as far as deep convection is considered. Here, we try to explore the role played by aerosols in modifying the sensible and latent heat fluxes during DCC formation.

To understand the effects of aerosols on sensible heat flux, simulation was carried out for period 27 August 2011 (00 GMT) to 29 August 2011 (07 GMT). Here two simulations are considered: the control run with original aerosol number concentration and the experiment run with aerosol number concentration reduced by 75%. The difference in sensible heat flux between the control run and the experiment run indicates the impact of aerosols on sensible heat flux. Figure 8 shows the domain-area averaged time series of differences in sensible heat fluxes between the control run and the experiment run.

In Fig. 8, we find that the difference is negative over most of the entire period, implying more sensible heat in the experiment run compared to the control run. When aerosols are reduced, less solar radiation is scattered and absorbed. Thus, more solar radiation reaches the surface. The increase in incoming solar flux induces increases in latent and sensible heat fluxes in the experiment run as compared to those fluxes in the control run. This maximum difference is observed at 14 GMT and is about 34 W m^{-2}. Subsequently, the difference is reduced possibly due to various dynamical feedbacks within the model.

Figure 9 shows spatial changes in sensible heat flux due to radiative and thermodynamic effects of aerosols. The difference is calculated by averaging the flux for the period in which the difference is observed to be high. We observe more sensible heat in the case where aerosols are reduced to one fourth of their actual concentration. Maximum flux with aerosols is about 270 W m^{-2}. When aerosol is reduced, the maximum flux is increased to 370 Wm^{-2}. The maximum difference observed is about 120 Wm^{-2}. The positive values of difference observed at certain grid points in Fig. 9c could be due to model dynamical and

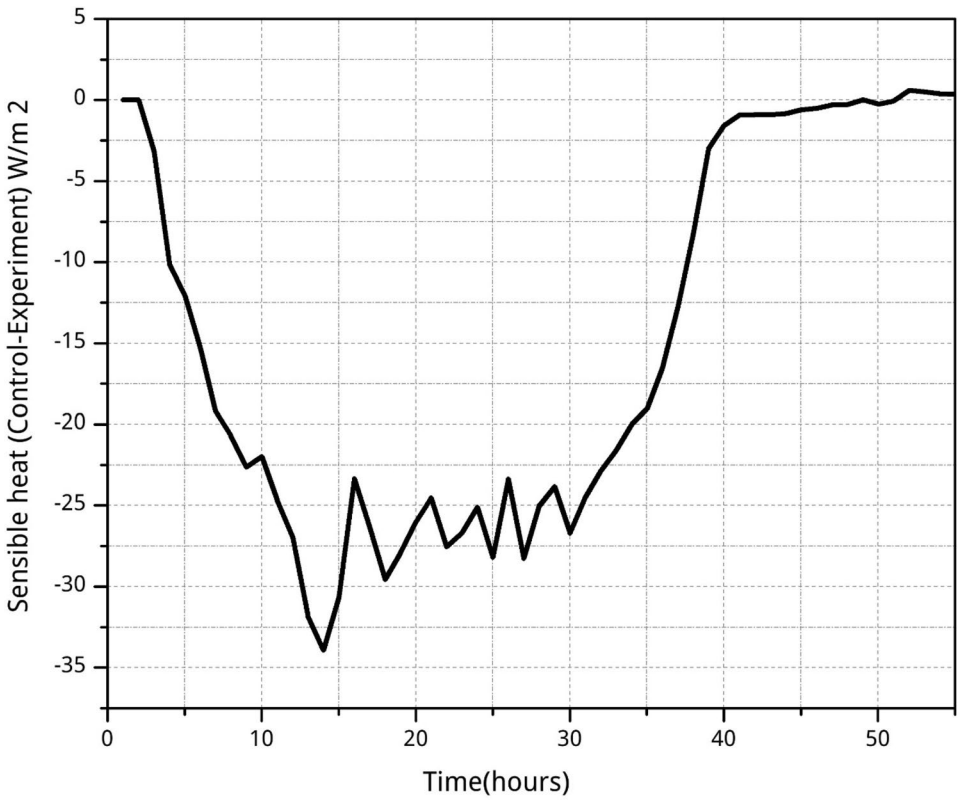

Fig. 8 Time series of area-averaged difference in sensible heat flux between the control run and the experiment run

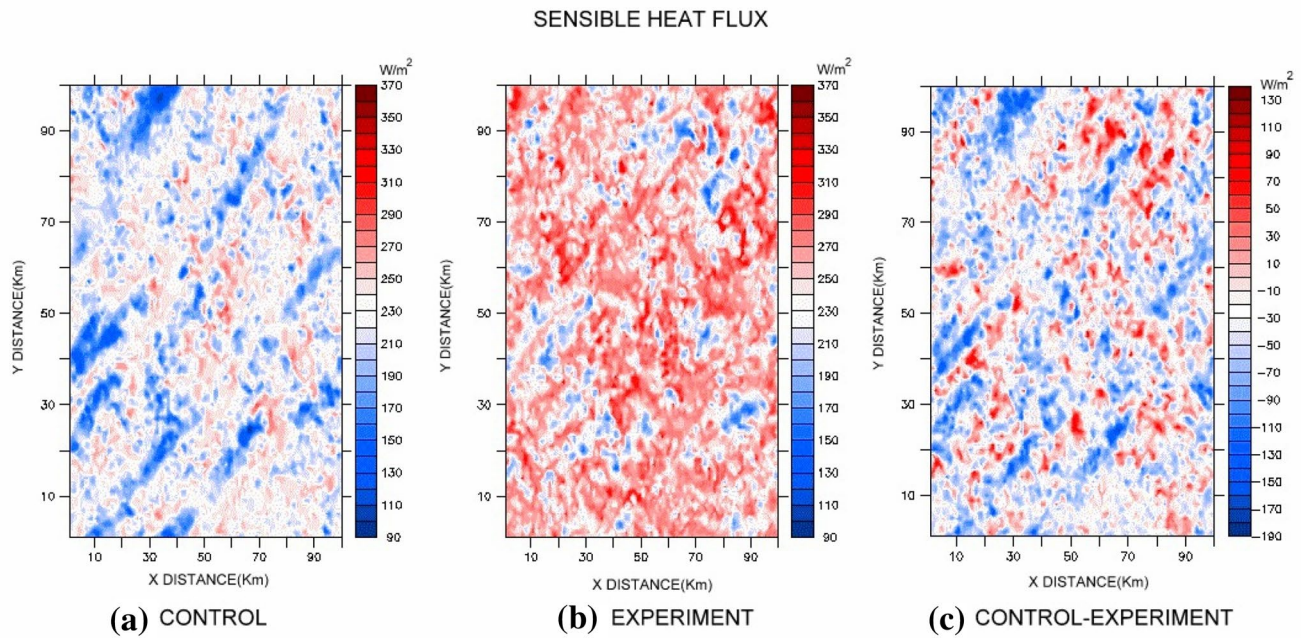

Fig. 9 Time-averaged plot of sensible heat flux simulated by model **a** control, **b** experiment and **c** difference between control and experiment runs

thermodynamical feedbacks arising due to non-linear processes. Upon area averaging, the difference is observed to be about 35 Wm^{-2}.

4.2 Effect on latent heat flux

Similar to Fig. 8, Fig. S5 illustrates the area-averaged time series of differences in latent heat fluxes between the control run and the experiment run. In Fig. 11 (which will be discussed in detail in Sect. 4.4), we find that for most of the period, the latent-heat difference is negative implying more latent heat in the experiment run than in the control run. The maximum difference is observed at 14 GMT on 28 August and is about 18 W m^{-2}. When aerosol concentration is reduced, the net incoming solar radiation is increased thus amplifying evaporation. This enhances evaporation and thus increases latent heat fluxes. The maximum flux in the control run is about 215 W m^{-2} (Fig. S6(a)), whereas in the experiment run, the maximum flux is about 250 W m^{-2} (Fig. S6(b)). Fig. S6(c) shows the change in latent heat flux due only to aerosols (Control minus Experiment). The maximum difference is about 100 Wm^{-2}. On taking the area average over differences in Fig. S6(c), the difference is about 90 Wm^{-2}. The more radiation reaching the surface in the experiment run could induce more evaporation of moisture from the surface, thereby enhancing latent heat flux. Latent heat flux could also be increased via the low-level convergence of moisture induced by aerosol heating of lower atmosphere (See Sect. 3.4).

4.3 Aerosol effect on lower atmospheric stability

Figure 10 shows the vertical profiles of differences in potential temperature between the experiment run and the control run, and stability in both of the runs at the Nainital location (29.4 N, 79.5 E). From earlier discussions, it is clear that aerosol reduces sensible heat fluxes at the surface. Reduced sensible heat fluxes can cool the surface and decrease surface temperature. In Fig. 10a, potential temperature is greater in the experiment run, wherein aerosol concentration is reduced. Thus, the difference in potential temperature between the control run and the experiment run yields negative values in lower levels, indicating a net cooling of the low-level atmosphere when aerosol concentration is enhanced. This low-level cooling is evident up to about 700 m. At the surface, cooling as high as 1.7 °C is observed.

In Fig. 10b, vertical gradient of potential temperature ($d\theta/dz$) is depicted. It is a measure of atmospheric stability. Higher values of $d\theta/dz$ indicate more stable atmosphere. From this figure, it is clear that stability is higher in the

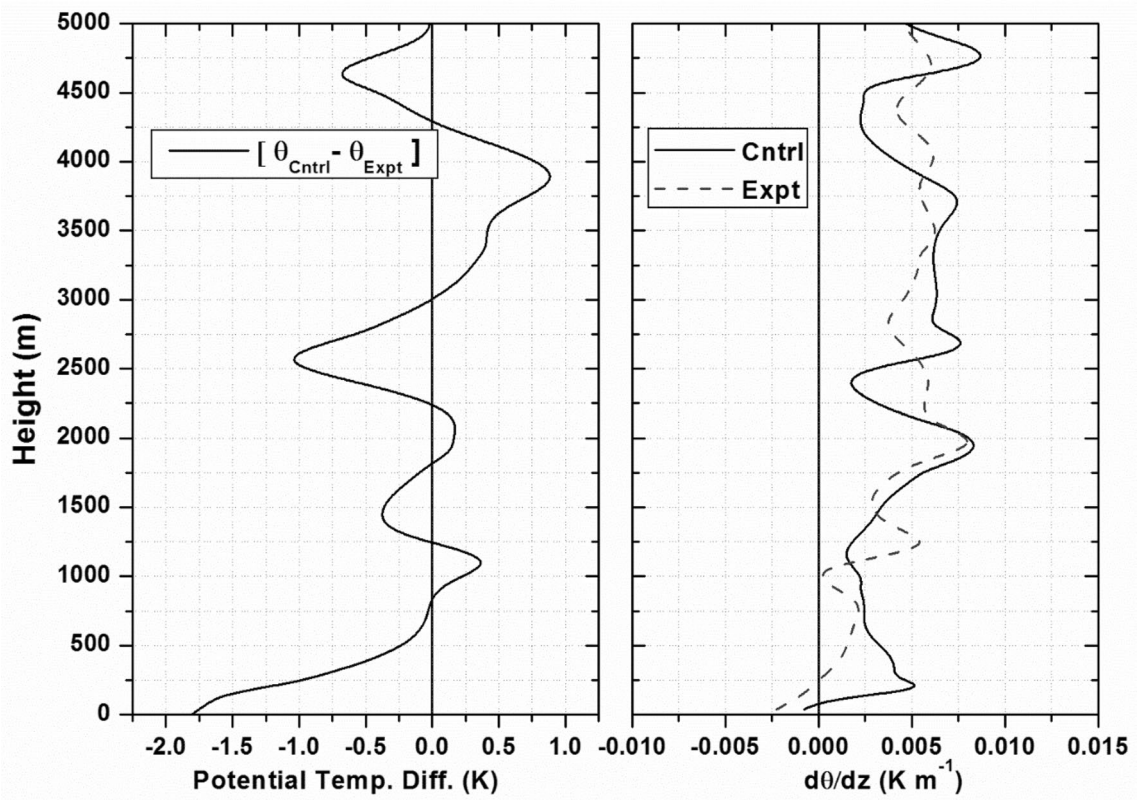

Fig. 10 **a** Vertical profile of potential temperature difference between control and experiment, **b** vertical profile of $d\theta/dz$

control run where aerosol concentration is higher particularly over the low-level atmosphere between the surface and 700 m. It is demonstrated that aerosols can enhance stability in the lower layers of atmosphere via surface cooling, which is in conformity with theoretical considerations. However, our findings suggest another possibility of overcoming this aerosol-induced stability via enhanced moisture convergence which needs to be considered explicitly.

4.4 Aerosol effect on deep convection

Development of deep convection is associated with a multitude of processes that either amplify or cancel one another, and depending on the feedback processes. Keeping in mind about these feedback processes, our next step is to investigate the role played by aerosols in enhancing deep convection. For development of deep convection, the lower troposphere heating and moistening are essential. Thus, we examine the moist static energy (MSE) which feasibly encompasses both temperature and moisture, as described in Sect. 3.4. In Fig. 11, we analyze the change in IE, LE and MSE, respectively, in the PBL (at 750 hPa level) for the control run and the experiment run. Figure 12 shows vertical profile of difference in IE, LE and MSE between the runs over Nainital.

In Fig. 11, the average difference between the fluxes in control run and the experiment run are produced and shown in the right column. It is seen that, to the region south and southwest of Nainital, the IE is greatly enhanced in the control run. The same pattern is observed for LE and MSE (Fig. 11b, c). In most of the regions, the differences in IE, LE, and MSE are positive implying that IE, LE and MSE are greater in the control run. The presence of absorbing aerosols in this region heats lower atmosphere and cause enhancement of IE, LE and MSE in the control run. Though it is expected that the lower stability is increased due to aerosols, it is shown that various dynamical and thermodynamical feedback can build up moist static energy making the atmosphere unstable. The thermo-dynamical response analyzed through MSE (Fig. 11c) arises primarily from IE

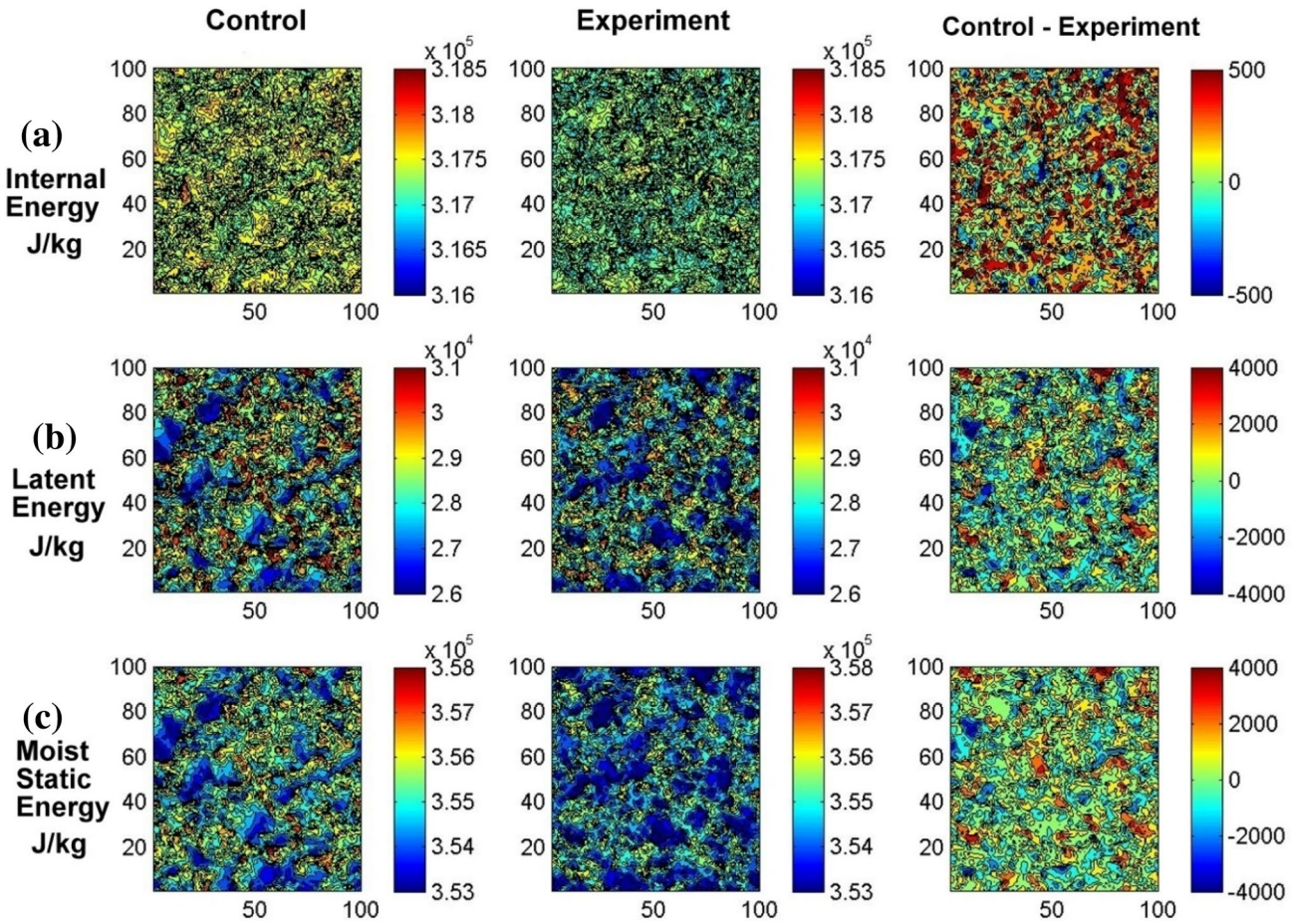

Fig. 11 Average spatial pattern of **a** internal energy (IE) in J kg^{-1} for the control, experiment, and difference between the control and experiment runs during 27-. **b** Same as **a** but for latent energy (LE) and **c** for moist-static energy (MSE). (The location of Nainital is exactly at the centre of each subplot)

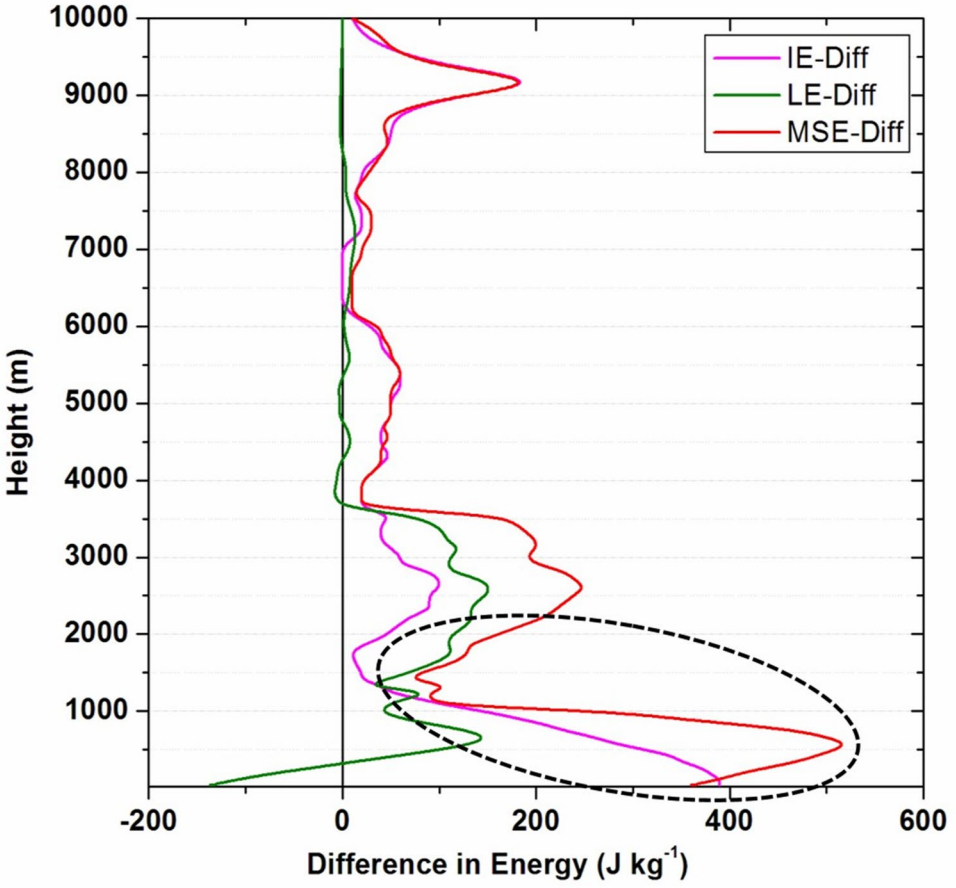

Fig. 12 Vertical profile of difference (control-experiment) of IE, LE, and MSE

(Fig. 11a) which is a function of temperature. However, there is a considerable contribution from the LE (Fig. 11b) as well. The same conclusion is evident in Fig. 12, wherein profiles are averaged spatially from a 100 km × 100 km box from the model centered at Nainital.

A confirmation of moisture convergence demonstrated in Sect. 3.4 is again performed here in the model simulation. Now we explore the vertical profile of composite of moisture convergence (MC) over the region which is essential for sustained deep convection.

Figure 13 shows moisture convergence for the control run and the experiment run which clearly indicates an enhanced MC at lower levels (PBL) for the control run (the left panel represents the MC for the control run and the experiment run, and the right panel portrays the difference in MC between the two runs., i.e., control minus experiment). Thus, our hypothesis is re-confirmed in the case of model experiment.

We also examine the accumulated rain obtained from the control run and the experiment run. Figure 14 gives precipitation averaged over domain for all time steps. From Fig. 14, it is evident that aerosol-induced moisture convergence and instability have resulted in excess rainfall in the control run. This implies that aerosols modify cloud properties in a way to result in the enhancement of precipitation.

5 Summary and conclusions

The competing aerosol-induced thermo-dynamical and microphysical effects are examined to characterize their relative roles in deep convection over the Indo-Gangetic Plain (IGP) region of the Indian subcontinent. The GVAX field campaign of ARM Project provided an opportunity to investigate the aerosol effects during the summer monsoon months (June through September) of 2011. The IGP region of the Indian subcontinent is of special interest as it hosts a variety of aerosol species and types, over a heterogeneous topography. Additionally, the anthropogenic influence over this area has been increasing, adding another dimension to the environmental change.

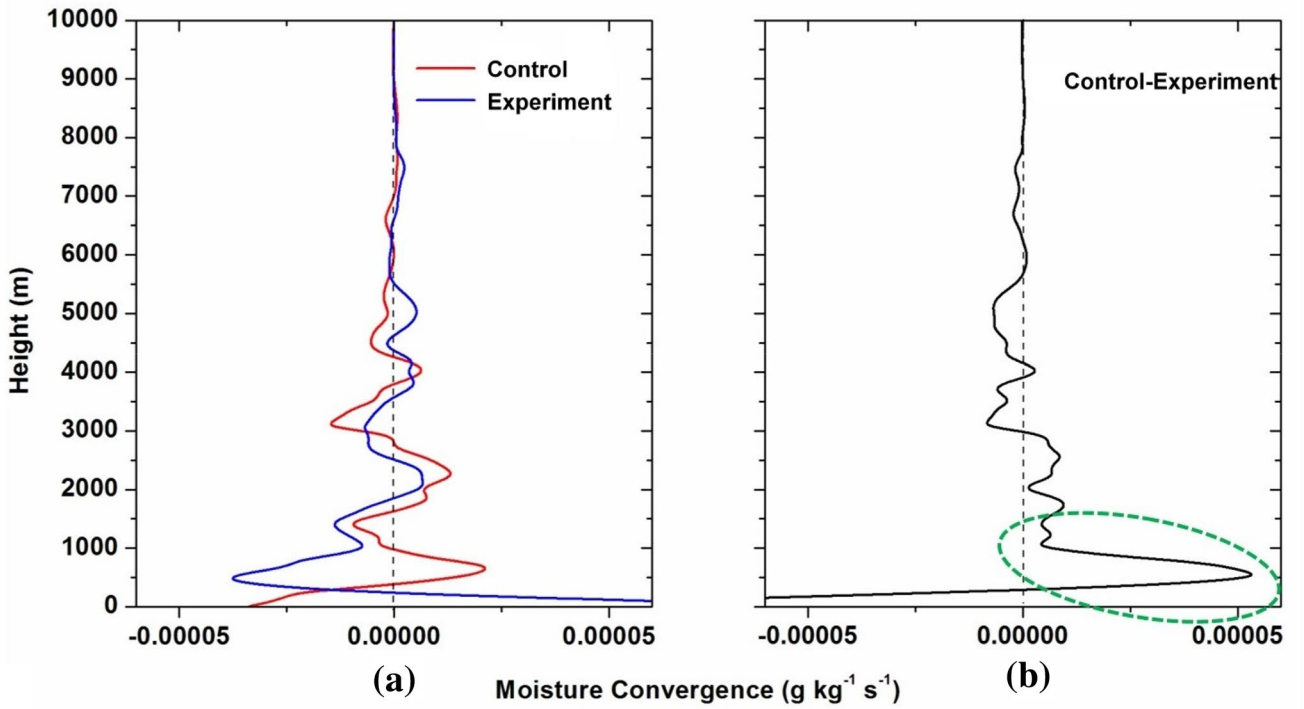

Fig. 13 Spatial mean of vertical profiles of moisture convergence for **a** the control and experiment runs, **b** difference in moisture convergence between the control and experiment runs

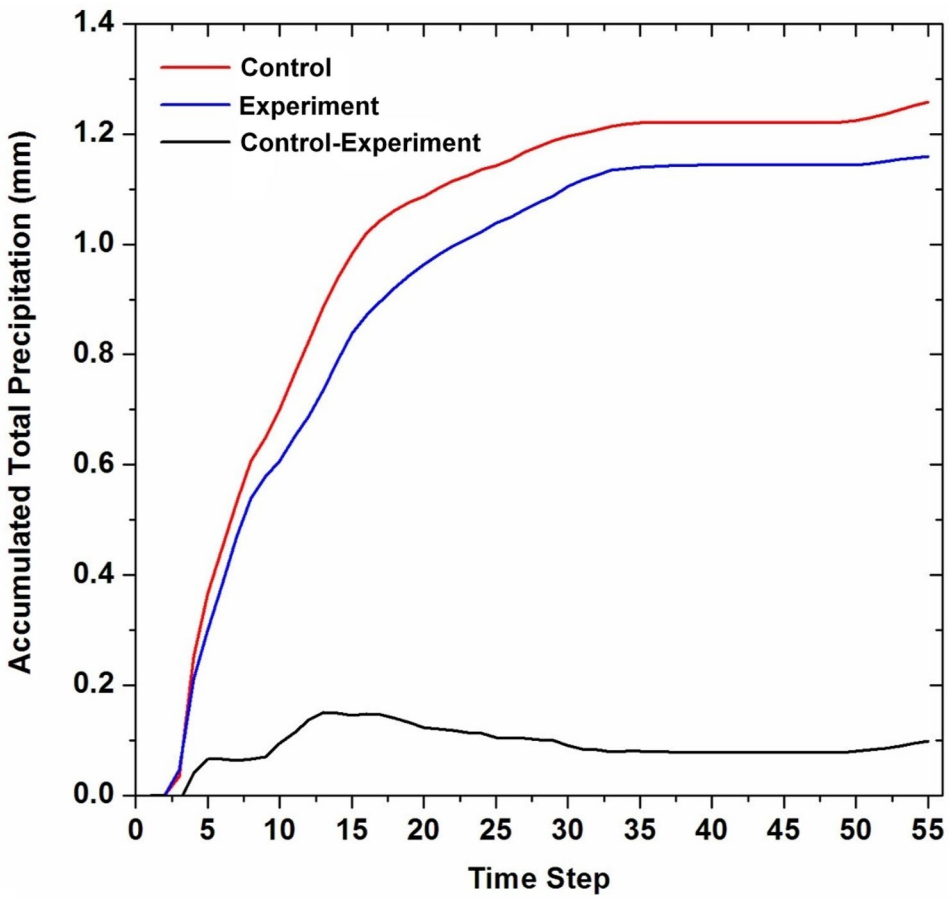

Fig. 14 Accumulated rainfall for the control run, experiment run and the difference between the runs

With a variety of satellite-, ground based-, and reanalysis- data of aerosol, cloud and meteorological parameters, it is demonstrated that the radiative effect of aerosols is significant in inducing a local warming. The aerosol radiative forcing and heating rate were estimated using a radiative transfer model with observed input variables. The atmospheric heating for the HADCC cases exhibits a clear-cut demarcation from that for the LADCC cases. An amplified aerosol-prompted warming at lower level stems from the heavy loading of absorbing aerosols during the occurrence of deep convection. Though it might lead to an aerosol-induced weakening of convection via the enhancement of stability in the PBL, mirrored in the form of reduced surface fluxes, it is overcome through another process in which the low-level MSE takes an upper hand. The MSE of the PBL is increased to a greater extent with increasing aerosol concentrations, primarily through an increase in its internal energy and secondly through a moist dynamic feedback which facilitates an enhancement of the latent energy through greater moisture convergence. Concurrently, the enhanced low-level moisture convergence destabilizes the column, thus creating an atmosphere conducive for intense convection and also enabling effective feedback with meteorology.

Further the role of microphysical processes is examined, however, a weakened invigoration is observed. This could be due to the domination of radiative effects over indirect microphysical influence. The WRF simulation of a deep convective event further isolates the aerosol effect, and substantiates our hypothesis. It is illustrated that the local stabilization is overcome primarily by an increase in the moist static energy. This increase is synchronized with a dynamical response in the form of greater low-level moisture convergence in association with enhanced atmospheric heating; and to some extent by the aerosol microphysical effects. This is a novel finding, as it suggests that the radiative impact of aerosols on deep convection is not restricted to local stabilization, but leads to regional dynamical changes that trigger greater moisture feedback and regional precipitation. However, it is underscored that a comprehensive effort by incorporating observations and model sensitivity tests are necessary to unravel the intricate feedbacks arising from radiative and microphysical processes under different environmental conditions.

Acknowledgements The authors wish to thank Ms. Maureen Cribb, Dr. Virginia Sawyer and Dr. Jianjun Liu for help with data management and processing. The data from ARM field campaign of US Department of Energy is also acknowledged. This work was supported by the US National Science Foundation (AGS1837811) and the Dept of Energy's ASR Program (DE-SC0018996), National Research Foundation of Korea (NRF) grant funded by the Korea government (MSIT) (No. NRF2020R1A2C1003215). This work was also supported by the "Construction of Ocean Research Stations and their Applicaton Studies" project, funded by the Ministry of Oceans and Fisheries (MOF), South Korea. The model used in our paper has been developed by the support by NRF (No. NRF2020R1A2C1003215) and MOF.

References

Albrecht BA (1989) Fractional cloudiness. Science 245(80):1227–1230

Andreae MO, Rosenfeld D, Artaxo P, Costa AA, Frank GP, Longo KM, Silva-Dias MAFD (2004) Smoking rain clouds over the Amazon. Science 303(5662):1337–1342

Babu SS, Satheesh SK, Moorthy KK (2002) Aerosol radiative forcing due to enhanced black carbon at an urban site in India. Geophys Res Lett 29(18):1880. https://doi.org/10.1029/2002GL015826

Back LE, Bretherton CS (2006) Geographic variability in the export of moist static energy and vertical motion profiles in the tropical Pacific. Geophys Res Lett 33:L17810. https://doi.org/10.1029/2006GL026672

Berg P, Moseley C, Haerter JO (2013) Strong increase in convective precipitation in response to higher temperatures. Nat Geosci 6:181–185. https://doi.org/10.1038/NGEO1731

Bhawar RL, Devara PCS (2010) Study of successive contrasting monsoons (2001–2002) in terms of aerosol variability over a tropical station Pune, India. Atmos Chem Phys 10:29–37

Bollasina M, Nigam S, Lau K-M (2008) Absorbing aerosols and summer monsoon evolution over south Asia: an observational portrayal. J Clim 21:3221–3239

Chakraborty A, Satheesh SK, Nanjundiah RS, Srinivasan J (2004) Impact of absorbing aerosols on the simulation of climate over the Indian region in an atmospheric general circulation model. Ann Geophys 22:1421–1434

Charlson RJ, Schwartz SE, Hales JM, Cess RD, Coakley JA, Hansen JE, Hofmann DJ (1992) Climate forcing by anthropogenic aerosols. Science 255:423–430

Chen F, Dudhia J (2001) Coupling an advanced land-surface hydrology model with the Penn State-NCAR MM5 modeling system. Part I: model description and implementation. Mon Weather Rev 129:569–585

Collier JC, Zhang GJ (2009) Aerosol direct forcing of the summer Indian monsoon as simulated by the NCAR CAM3. Clim Dyn 32:313–332. https://doi.org/10.1007/s00382-008-0464-9

CTCZ (Continental Tropical Convergence Zone Programme (2011): Science Plan. Department of Science and Technology, Government of India, New Delhi. ISBN No. 978–81–7525–997–3

d'Almedia GA, Koepke P, Shettle EP (1991) Atmospheric aerosols: global climatology and radiative characteristics. Deepak Publishing, Hampton

Dey S, Tripathi SN (2007) Estimation of aerosol optical properties and radiative effects in the Ganga basin, northern India, during the wintertime. J Geophys Res 112:D03203. https://doi.org/10.1029/2006JD007267

Donner LJ, Phillips VT (2003) Boundary layer control on convective available potential energy: Implications for cumulus parameterization. J Geophys Res Atmos 108(D22)

Fan J, Yuan T, Comstock JM, Ghan S, Khain A, Leung LR, Li Z, Martins VJ, Ovchinnikov M (2009) Dominant role by vertical wind shear in regulating aerosol effects on deep convective clouds. J Geophys Res Atmos 114:D22206. https://doi.org/10.1029/2009JD012352

Fan J, Rosenfeld D, Zhang Y, Giangrande SE, Li Z et al (2018) Substantial convection and precipitation enhancements by ultrafine aerosol particles. Science 359:411–418. https://doi.org/10.1126/science.aan8461

Feingold G, Remer LA, Ramaprasad J, Kaufman YJ (2001) Analysis of smoke impact on clouds in Brazilian biomass burning regions:

an extension of Twomey's approach. J Geophys Res Atmos 106(D19):22907–22922
Fouquart Y, Bonnel B (1980) Computation of solar heating of the Earth's atmosphere: a new parameterization. Beitr Phys Atmos 53:35–62
van Den Heever SC, Cotton WR (2007) Urban aerosol impacts on downwind convective storms. J Appl Meteorol Climatol 46(6):828–850
Hess SL (1979) An Introduction to Theoretical Meteorology, Krieger Publishing Co
Hsu NC, Herman JR, Gleason JF, Torres O, Seftor CJ (1999) Satellite detection of smoke aerosols over a snow/ice surface by TOMS. Geophys Res Lett 26:1165–1168. https://doi.org/10.1029/1999GL900155
IPCC, Intergovernmental Panel on Climate Change (2007) WG1/TAR07, http://www.grida.no/climate/ipcc_tar/wg1/pdf/tar-07.pdf
Jai Devi J, Tripathi SN, Gupta T, Singh BN, Gopalakrishnan V, Dey S (2011) Observation-based 3-D view of aerosol radiative properties over Indian Continental Tropical Convergence Zone: implications to regional climate. Tellus 63B:971–989
Kaskaoutis DG, Houssos EE, Solmon F, Legrand M, Rashki A, Dumka UC, Francois P, Gautam R, Singh RP (2018) Impact of atmospheric circulation types on southwest Asian dust and Indian summer monsoon rainfall. Atmos Res 201:189–205. https://doi.org/10.1016/j.atmosres.2017.11.002
Khain A, Pokrovsky A, Pinsky M, Seifert A, Phillips V (2004) Simulation of effects of atmospheric aerosols on deep turbulent convective clouds using a spectral microphysics mixed-phase cumulus cloud model. Part I: Model description and possible applications. J Atmos Sci 61(24):2963–2982
Khain A, Rosenfeld D, Pokrovsky A (2005) Aerosol impact on the dynamics and microphysics of deep convective clouds. Q J R Meteorol Soc 131(611):2639–2663
Koepke P, Hess M, Schult I, Shettle EP (1997) Global aerosol dataset. Max-Plank-Institut für Meteorologie Report 243:44
Koren I, Kaufman YJ, Rosenfeld D, Remer LA, Rudich Y (2005) Aerosol invigoration and restructuring of Atlantic convective clouds. Geophys Res Lett 32:L14828. https://doi.org/10.1029/2005GL023187
Lau K-M, Kim MK, Kim KM (2006) Asian summer monsoon anomalies induced by aerosol direct forcing: the role of the Tibetan Plateau. Clim Dyn 26:855–864
Lau WKM, Kim K-M, Hsu CN, Holben BN (2009) Possible influences of air pollution, dust- and sandstorms on the Indian monsoon, WMO Bulletin (Weather, Climate, Water), Volume 58(1) - January 2009, (http://www.wmo.int/pages/publications/bulletin_en/archive/58_1_en/58_1_lau_en.html)
Lee SS, Penner JE, Saleeby SM (2009) Aerosol effects on liquid-water path of thin stratocumulus clouds. J Geophys Res 114:D07204. https://doi.org/10.1029/2008JD010513
Lee S-S, Feingold G (2010) Precipitating cloud-system response to aerosol perturbations. Geophys Res Lett 37:L23806. https://doi.org/10.1029/2010GL045596
Lee S-S, Feingold G (2013) Aerosol effects on the cloud-field properties of tropical convective clouds. Atmos Chem Phys 13:6713–6726. https://doi.org/10.5194/acp-13-6713-2013
Lee S-S, Donner LJ, Penner JE (2010) Thunderstorm and stratocumulus: how does their contrasting morphology affect their interactions with aerosols? Atmos Chem Phys 10(14):6819
Li Z, Niu F, Fan J, Liu Y, Rosenfeld D, Ding Y (2011) The long-term impacts of aerosols on the vertical development of clouds and precipitation. Nature GeoSci. https://doi.org/10.1038/NGEO1313
Li Z et al (2016) Aerosol and monsoon interactions in Asia. Geophys, Rev. https://doi.org/10.1002/2015RG000500
Li Z, Rosenfeld D, Fan J (2017a) Aerosols and their impact on radiation, clouds, precipitation, and severe weather events. Oxford Res Encycl. https://doi.org/10.1093/acrefore/9780199389414.013.126
Li Z, Guo J, Ding A, Liao H, Liu J, Sun Y, Wang T, Xue H, Zhang H, Zhu B (2017b) Aerosols and boundary-layer interactions and impact on air quality. Natl Sci Rev 4:810–833. https://doi.org/10.1093/nsr/nwx117
Li Z, Wang Y, Guo J, Zhao C, Cribb MC, Dong X et al (2019) East asian study of tropospheric aerosols and their impact on regional clouds, precipitation, and climate (EAST-AIRCPC). J Geophy Res Atmos 124:13026–13054. https://doi.org/10.1029/2019JD030758
Maloney ED (2009) The moist static energy budget of a composite tropical intraseasonal oscillation in a climate model. J Clim 22(3):711–729. https://doi.org/10.1175/2008JCLI2542.1
Manabe S, Holloway JL, Stone HM (1970) Tropical circulation in a time-integration of a global model of the atmosphere. J Atmos Sci 27:580–613. https://doi.org/10.1175/1520-0469(1970)027%3c0580:TCIATI%3e2.0.CO;2
Manoj MG, Devara PCS, Safai PD, Goswami BN (2011) Absorbing aerosols facilitate transition of Indian monsoon breaks to active spells. Clim Dyn 37(11–12):2181–2198
Manoj MG, Devara PCS, Joseph S, Sahai AK (2012) Aerosol indirect effect during the aberrant Indian Summer Monsoon breaks of 2009. Atmos Environ 60:153–163
Medeiros B, Hall A, Stevens B (2005) What controls the mean depth of the PBL? J Clim 18:3157–3172
Menon S (2004) Current uncertainties in assessing aerosol effects on climate. Annu Rev Environ Resour 29:1–30. https://doi.org/10.1146/annurev.energy.29.063003.132549
Menon S, Hansen JE, Nazarenko L, Luo Y (2002) Climate effects of black carbon aerosols in China and India. Science 297:2250–2253. https://doi.org/10.1126/science.1075159
Mlawer EJ, Taubman SJ, Brown PD, Iacono MJ, Clough SA (1997) RRTM, a validated correlated-k model for the longwave. J Geophys Res 102:16663–21668
Niu F, Li Z (2012) Systematic variations of cloud top temperature and precipitation rate with aerosols over the global tropics. Atmos Chem Phys. https://doi.org/10.5194/acp-12-8491-2012
Pandithurai G, Pinker RT, Takamura T, Devara PCS (2004) Aerosol radiative forcing over a tropical urban site in India. Geophys Res Lett 31:L12107. https://doi.org/10.1029/2004GL019702
Peng J, Li Z, Zhang H, Liu J, Cribb MC (2016) Systematic changes in cloud radiative forcing with aerosol loading for deep clouds from multi-year global A-Train satellite datasets. J Atmos Sci 73:231–249. https://doi.org/10.1175/JAS-D-15-0080.1
Rafkin SCR (2012) The potential importance of non-local, deep transport on the energetics, momentum, chemistry, and aerosol distributions in the atmospheres of Earth, Mars and Titan. Planet Space Sci 60(1):147–154
Rajeevan M, Gadgil S, Bhate J (2010) Active and break spells of the Indian summer monsoon. J Earth Sys Sci 119(3):229–247
Ramanathan V et al (2013) Black Carbon and the Regional Climate of California. Report to the California Air Resources Board Contract 08–323. www.arb.ca.gov/research/rsc/3-8-13/item8dfr08-323.pdf
Ramanathan V, Carmichael G (2008) Global and regional climate changes due to black carbon. Nat Geosci 1:221–227
Ramanathan V, Chung C, Kim D, Bettge T, Buja L, Kiehl JT, Washington WM, Fu Q, Sikka DR, Wild M (2005) Atmospheric brown clouds: impacts on south Asian climate and hydrological cycle. Proc Nat Acad Sci 102(15):5326–5333
Ravi Kiran V, Rajeevan M, Vijaya Bhaskara Rao S, Prabhakara Rao N (2009) Analysis of variations of cloud and aerosol properties associated with active and break spells of Indian summer monsoon using MODIS data. Geophys Res Lett 36:L09706. https://doi.org/10.1029/2008GL037135

Ricchiazzi P, Yang S, Gautier C, Sowle D (1998) SBDART: a research and teaching software tool for plane-parallel radiative transfer in the Earth's atmosphere. Bull Am Meteor Soc 79:2101–2114

Rochetin N, Couvreux F, Grandpeix JY, Rio C (2014) Deep convection triggering by boundary layer thermals. Part I: LES analysis and stochastic triggering formulation. J Atmos Sci 71(2):496–514

Rosenfeld D, Woodley WL (2000) Deep convective clouds with sustained supercooled liquid water down to −37.5 °C. Nature 405:440–442

Rosenfeld D, Lohmann U, Raga GB, O'Dowd CD, Kulmala M, Fuzzi S, Reissell A, Andreae MO (2008) Flood or drought: how do aerosols affect precipitation? Science 321(5894):1309–1313. https://doi.org/10.1126/science.1160606

Rosenfeld D, Wood R, Donner LJ, Sherwood SC (2013) Aerosol cloud-mediated radiative forcing: Highly uncertain and opposite effects from shallow and deep clouds, Chapter 5. In: Climate Science for Serving Society: Research, Modeling and Prediction Priorities (Eds: Asrar GR, Hurrell JW). Springer, New York

Rosenfeld D, Zhu Y, Wang M, Zheng Y, Goren T, Yu S (2019) Aerosol-driven droplet concentrations dominate coverage and water of oceanic low-level clouds, Science, 363, 599: 1–9, eaav0566, doi: https://doi.org/10.1126/science.aav0566

Rossow WB, Schiffer RA (1999) Advances in understanding clouds from ISCCP. Bull Am Meteorol Soc 80(11):2261–2288

Saleeby SM, Cotton WR (2004) A large-droplet mode and prognostic number concentration of cloud droplets in the Colorado state university regional atmospheric modeling system (RAMS). Part I: Module description and supercell test simulations. J Appl Meteorol 43:182–195

Sawyer V, Li Z (2013) Detection, variations and intercomparison of the planetary boundary layer depth from radiosonde, lidar and infrared spectrometer. Atmos Environ 79:518–528

Shamanaev VS, Kokhanenko GP (2013) Vertical distribution of aerosol mass concentration in the atmospheric boundary layer above the Atlantic Ocean from lidar sensing data. Russ Phys J 56(3):269–272

Singh C, Ganguly D, Dash SK (2018) On the dust load and rainfall relationship in South Asia: an analysis from CMIP5. Clim Dyn 50:403–422. https://doi.org/10.1007/s00382-017-3617-x

Singh C, Ganguly D, Sharma P (2019) Impact of West Asia, Tibetan Plateau and local dust emissions on intra-seasonal oscillations of the South Asian monsoon rainfall. Clim Dyn 53:6569–6593. https://doi.org/10.1007/s00382-019-04944-5

Skamarock WC, Klemp JB, Dudhia J, Gill DO, Barker DM, Wang W, Powers JG (2008) A description of the advanced research WRF version 3 (No. NCAR/TN-475+STR), University Corporation for Atmospheric Research. https://doi.org/10.5065/D68S4MVH

Steiner AL, Mermelstein D, Cheng SJ, Twine TE, Oliphant A (2013) Observed impact of atmospheric aerosols on the surface energy budget. Earth Interact 17:1–22. https://doi.org/10.1175/2013EI000523.1

Stull RB (1988) An introduction to boundary layer meteorology. Springer, New York, p 666

Su T, Li Z, Li C, Li J, Han W, Shen C, Tan W, Wei J, Guo J (2020) The significant impact of aerosol vertical structure on lower atmosphere stability and its critical role in aerosol–planetary boundary layer (PBL) interactions. Atmos Chem Phys 20(3713–3724):2020. https://doi.org/10.5194/acp-20-3713-2020

Tao W-K, Li X, Khain A, Matsui T, Lang S, Simpson J (2007) Role of atmospheric aerosol concentration on deep convective precipitation: cloud-resolving model simulations. J. Geophys. Res. 112:D24S18. https://doi.org/10.1029/2007JD008728

Tao W-K, Chen J-P, Li Z, Wang C, Zhang C (2012) Impact of aerosols on convective clouds and precipitation. Rev Geophys 50: RG2001. https://doi.org/10.1029/2011RG000369

Tripathi SN, Tare V, Chinnam N, Srivastava AK, Dey S, Agarwal A, Kishore S, Lal RB, Manar M, Kanawade VP, Chauhan SSS, Sharma M, Reddy RR, Gopal KR, Narasimhulu K, Reddy LSS, Gupta S, Lal S (2006) Measurements of atmospheric parameters during Indian Space Research Organization Geosphere Biosphere Program Land Campaign II at a typical location in the Ganga Basin: 1. Physical and optical properties. J Geophys Res 111:D23209. https://doi.org/10.1029/2006JD007278

Wang C, Kim D, Ekman AML, Barth MC, Rasch PJ (2009) Impact of anthropogenic aerosols on Indian summer monsoon. Geophys Res Lett 36:L21704. https://doi.org/10.1029/2009GL040114

Wu X, Deng L (2013) Comparison of moist static energy and budget between the GCM-simulated Madden–Julian Oscillation and observations over the Indian Ocean and Western Pacific. J Clim 26(14):4981–4993. https://doi.org/10.1175/JCLI-D-12-00607.1

Xu K-M, Cederwall RT, Donner LJ et al (2002) An intercomparison of cloud-resolving models with the Atmospheric Radiation Measurement summer 1997 Intensive Observation Period data. Quart J Roy Meteorol Soc 128:593–624

Yan H, Li Z, Huang J, Cribb MC, Liu J (2014) Long-term aerosol-mediated changes in cloud radiative forcing of deep clouds at the top and bottom of the atmosphere over the Southern Great Plains. Atmos Chem Phys. https://doi.org/10.5194/acp-14-7113-2014

Zhang W, Augustin M, Zhang Y, Li Z, Xu H, Liu D et al (2015) Spatial and temporal variability of aerosol vertical distribution based on lidar observations: a haze case study over Jinhua basin. Adv Meteorol 349592:1–8. https://doi.org/10.1155/2015/349592

Zhou X, Geerts B (2013) The influence of soil moisture on the planetary boundary layer and on cumulus convection over an isolated mountain. Part I: Observations. Mon Weather Rev 141(3):1061–1078